Article

Cell Reports

Diet-Induced Growth Is Regulated via Acquired Leptin Resistance and Engages a Pomc-Somatostatin-Growth Hormone Circuit

Graphical Abstract

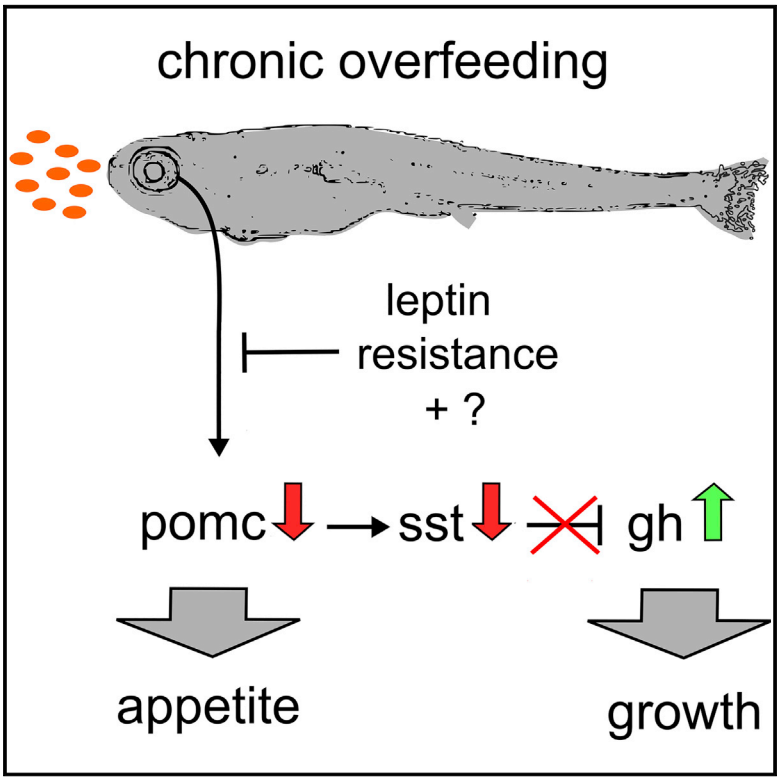

Highlights

- Sst neurons are second-order neurons of the central melanocortin system
- Pomc neurons stimulate Sst neurons, resulting in reduced growth hormone levels
- Excessive feeding leads to leptin resistance and decreased *pomc* expression
- Reduced *pomca* transcription favors somatic growth when food resources are plentiful

Authors

Heiko Löhr, Simon Hess, Mafalda M.A. Pereira, ..., Peter Kloppenburg, Jens C. Brüning, Matthias Hammerschmidt

Correspondence

mhammers@uni-koeln.de

In Brief

The melanocortin system controls energy homeostasis and somatic growth, but the underlying mechanisms are elusive. Löhr et al. identify a functional neural circuit in which Pomc neurons stimulate hypothalamic somatostatin neurons, thereby inhibiting hypophyseal growth hormone production. Excessive feeding and acquired leptin resistance attenuate this pathway, allowing faster somatic growth when food resources are rich.

Löhr et al., 2018, Cell Reports *23*, 1728–1741
May 8, 2018
https://doi.org/10.1016/j.celrep.2018.04.018

CellPress

OPEN ACCESS
CellPress

Cell Reports
Article

Diet-Induced Growth Is Regulated via Acquired Leptin Resistance and Engages a Pomc-Somatostatin-Growth Hormone Circuit

Heiko Löhr,[1] Simon Hess,[1] Mafalda M.A. Pereira,[2] Philip Reinoß,[1] Sandra Leibold,[1] Christel Schenkel,[1] Claudia M. Wunderlich,[2] Peter Kloppenburg,[1,3] Jens C. Brüning,[2,3,4] and Matthias Hammerschmidt[1,3,4,5,*]
[1]Institute of Zoology, University of Cologne, Cologne, Germany
[2]Department of Neuronal Control of Metabolism, Max Planck Institute for Metabolism Research, Cologne, Germany
[3]Cologne Excellence Cluster on Cellular Stress Responses in Aging-Associated Diseases, University of Cologne, Cologne, Germany
[4]Center for Molecular Medicine Cologne, University of Cologne, Cologne, Germany
[5]Lead Contact
*Correspondence: mhammers@uni-koeln.de
https://doi.org/10.1016/j.celrep.2018.04.018

SUMMARY

Anorexigenic pro-opiomelanocortin (Pomc)/alpha-melanocyte stimulating hormone (αMSH) neurons of the hypothalamic melanocortin system function as key regulators of energy homeostasis, also controlling somatic growth across different species. However, the mechanisms of melanocortin-dependent growth control still remain ill-defined. Here, we reveal a thus-far-unrecognized structural and functional connection between Pomc neurons and the somatotropic hypothalamo-pituitary axis. Excessive feeding of larval zebrafish causes leptin resistance and reduced levels of the hypothalamic satiety mediator *pomca*. In turn, this leads to reduced activation of hypophysiotropic somatostatin (Sst)-neurons that express the melanocortin receptor Mc4r, elevated growth hormone (GH) expression in the pituitary, and enhanced somatic growth. Mc4r expression and αMSH responsiveness are conserved in Sst-expressing hypothalamic neurons of mice. Thus, acquired leptin resistance and attenuation of *pomca* transcription in response to excessive caloric intake may represent an ancient mechanism to promote somatic growth when food resources are plentiful.

INTRODUCTION

Excessive energy intake is associated with obesity and increased linear growth, suggesting a coordinated interplay between systems controlling energy homeostasis and the somatotropic axis (He and Karlberg, 2001; Savastano et al., 2014). A key neuroendocrine network involved in regulating food intake and metabolism in vertebrates is the melanocortin (MC) circuitry of the hypothalamus (Krashes et al., 2016; Timper and Brüning, 2017). Here, two antagonistic neuronal populations of the arcuate nucleus, releasing either Agouti-related peptide (Agrp) or the Pomc-derived peptide alpha-melanocyte stimulating hormone (αMSH), sense the energy state of the organism via hormonal and nutritional signals from the periphery, including leptin, or are regulated by centrally derived signals (Chen et al., 2015; Garfield et al., 2016). αMSH binds and activates melanocortin 4 receptor (Mc4r) expressed on distinct second-order neurons and conveys anorexigenic responses (decreased food uptake and increased energy expenditure), whereas the orexigenic peptide Agrp functions as an antagonist or inverse agonist of Mc4r. Pomc and Agrp neurons form extensive projections throughout the brain, including main target areas involved in energy homeostasis control, such as the paraventricular nucleus (PVN) of the hypothalamus (King and Hentges, 2011; Wang et al., 2015). In mammals, genetic loss of leptin (Zhang et al., 1994), Pomc (Yaswen et al., 1999), or Mc4r (Huszar et al., 1997) function leads to severe obesity (Krashes et al., 2016; Timper and Brüning, 2017). Diet-induced obesity in genetically unaffected individuals can be enhanced by a phenomenon called acquired leptin resistance, with reduced leptin receptor signal transduction in, and reduced activation of, Pomc cells despite high leptin serum levels. While the exact molecular mechanisms underlying this phenomenon are elusive, they appear to involve an overactivation of cell-autonomous negative feedback responses (Enriori et al., 2007; Friedman, 2014, 2016; O'Rahilly, 2014).

In addition to obesity, loss-of-function mutations in Pomc or Mc4r also result in moderately enhanced linear growth both in rodents (Huszar et al., 1997; Yaswen et al., 1999) and humans (Farooqi et al., 2000; Krude et al., 2003; Martinelli et al., 2011). Somatic growth is primarily regulated via growth hormone (GH) released by somatotrophes in the adenohypophysis of the pituitary gland. GH expression and release by somatotrophes is inhibited by Sst-expressing neurons of the periventricular nucleus (PeVN) and PVN, while hypothalamic GH-releasing hormone (Ghrh)-expressing neurons have opposite effects on GH (Tauber and Rochiccioli, 1996; Eigler and Ben-Shlomo, 2014). However, the molecular basis of melanocortin-dependent control of somatic growth remains enigmatic, and neither Sst nor Ghrh cells had been identified as second-order neurons of the melanocortin system as yet.

In zebrafish, the somatotropic and melanocortin systems are remarkably conserved. Similar to mammals, zebrafish GH (*gh1*)-expressing cells are located in the zebrafish adenohypophysis, and *gh1* mutants display strongly decreased somatic

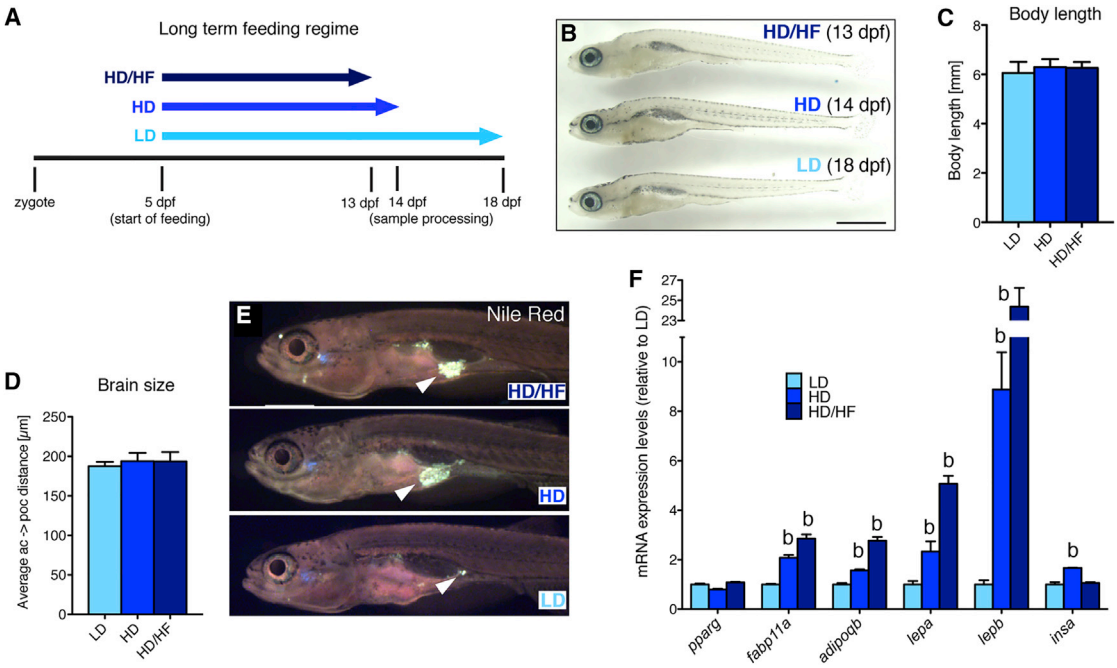

Figure 1. Effects of Long-Term Caloric Excess on Linear Growth and Lipid Metabolism in Larval Zebrafish

(A) Feeding paradigm for generation of size-matched zebrafish larvae with different caloric energy input (see text for details). Samples were collected at a standard body length of 6 mm at 13 dpf (HD/HF), 14 dpf (HD), and 18 dpf (LD).

(B) Lateral view of treated larvae.

(C and D) Quantification of body length (n = 20 for each group) (C) and distance between anterior and postoptic commissures as a measure for brain size (D) in *pomca:EGFPras* transgenic fish (see Figure 3; n = 10).

(E) Nile red staining of visceral lipids (arrowheads).

(F) qRT-PCR analyses of mRNA levels for *pparg*, *fabp11a*, *adipoqb*, *lepa*, *lepb*, and *insa*.

Scale bar in (B) represents 1 mm. b, $p < 0.01$ relative to respective LD groups (F). Error bars in (C), (D), and (F) show SD.

growth (McMenamin et al., 2013), whereas the neuroanatomy and function of Sst and Ghrh neurons in the context of somatic growth have not been studied in this species. Moreover, zebrafish Pomca and Agrp neurons are located in hypothalamic domains homologous to the mammalian arcuate nucleus (Forlano and Cone, 2007), and studies in different teleost species suggest a conserved function of the melanocortin system in control of energy homeostasis (Cerdá-Reverter et al., 2011). In addition, the zebrafish melanocortin system affects somatic growth; transgenic overexpression of Agrp results in increased *gh1* expression and body length (Song and Cone, 2007), whereas morpholino-based *agrp* knockdown has opposite effects (Zhang et al., 2012). These effects were assigned to a direct innervation of the adenohypophysis by Pomc and Agrp neurons (Zhang et al., 2012) rather than involving Sst neurons as mediators.

Here, we provide first evidence for the existence and functionality of such a Pomc-Sst-Gh axis in zebrafish and mouse regulating somatic growth dependent of caloric energy availability.

RESULTS

Long-Term Caloric Excess Increases Growth Rate and Lipid Metabolism of Larval Zebrafish

In order to analyze the interplay between energy supply and linear growth during zebrafish development, we applied different feeding conditions to zebrafish larvae starting at 5 days post-fertilization (dpf): (1) low-density suspension of live paramecia representing limited food resources (LD), (2) high-density paramecia suspension representing *ad libitum* feeding conditions (HD), and (3) HD paramecia plus additional daily supply of egg yolk representing *ad libitum*/high-fat diet conditions (HD/HF). Such differences in feeding regimes affected not only linear/somatic growth but also the developmental pace of larvae, as judged by anatomical staging (Parichy et al., 2009) (Figures S1A–S1C and S1N–S1V) and similar to what has been shown in juvenile fish (Leibold and Hammerschmidt, 2015). Therefore, comparative analyses were performed not only between age-matched larvae (15 dpf) of different sizes (Figures S1A–S1M) but also primarily between size-matched larvae of a standard length of 6 mm (Figures 1A–1D), which was obtained at 13 dpf for HD/HF, 14 dpf for HD, and 18 dpf for LD larvae, respectively. Examination of visceral neutral lipid droplets by Nile red staining revealed larger lipid depots in the HD and HD/HF groups than in the LD group (Figure 1E). Consistently, HD and HD/HF larvae displayed moderately increased expression of fatty acid binding protein 11a (*fabp11a*), a marker for differentiated adipocytes (Imrie and Sadler, 2010), and of the adipokine adiponectin b (*adipoqb*), and strongly increased expression of the two leptin paralogs *lepa* and *lepb*. In contrast, expression of peroxisome

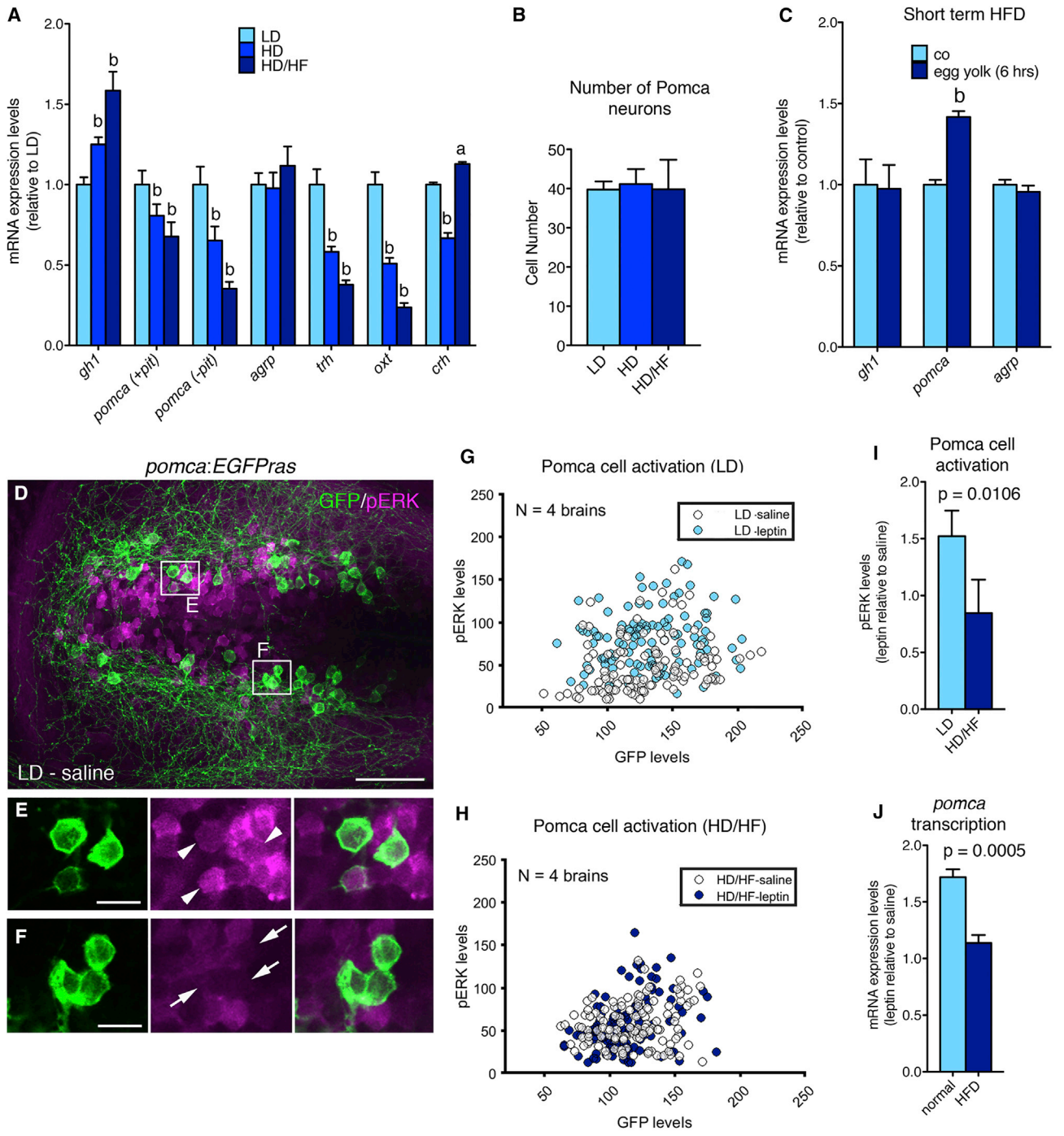

Figure 2. Long-Term Overfeeding Causes Leptin Resistance and Has an Impact on Both the Melanocortin and GH Systems

(A) qRT-PCR analyses of mRNA levels for *gh1*, *pomca*, *agrp*, *trh*, *oxt*, and *crh*. Corticotropin-releasing hormone (Dhillo et al., 2002) (*crh*) was downregulated in the HD group, but not in the HD/HF group, possibly pointing to stress responses caused by incubation in egg yolk medium. To specifically assess hypothalamic *pomca* expression levels, the pituitary was removed in *pomca* (−pit).

(B) Number of Pomca neurons in three feeding groups as determined by anti-GFP IF and cell counts in *pomca:EGFPras* fish (see Figure 3; n = 10).

(C) mRNA levels of *gh1*, *pomca*, and *agrp* after short-term application of egg yolk to 14 dpf larvae.

(D–F) IF for GFP and pERK on an exemplary *pomca:EGPras* transgenic larval brain (see Figure 3) subjected to the LD feeding regimen and incubated in saline.

(D) Overview of hypothalamic regions with GFP+/pERK+ domains.

(E and F) Magnification of areas boxed in (D) revealing GFP+/pERK+ cells (E, arrowheads) and GFP+/pERK- cells (F, arrows).

(legend continued on next page)

proliferator-activated receptor gamma (*pparg*), marking both developing and mature adipocytes (Gesta et al., 2007), was unaltered (Figure 1F). Since obesity is commonly associated with hyperinsulinemia, we also analyzed insulin (*insa*) expression and found increased *insa* expression in the HD group, but not in the HD/HF group, compared to the LD control (Figure 1F). Together, this indicates that long-term high fat-diet promoted both somatic growth and obesity, but not necessarily hyperinsulinemia.

Long-Term Caloric Excess Causes Leptin Resistance and Affects Both the Melanocortin and GH System

We also assessed transcript levels of *gh1* and the two melanocortin peptides *pomca* and *agrp* (Figure 2A). *gh1* levels were significantly elevated in the HD and HD/HF groups compared to the LD group. In contrast, *agrp* levels were similar in all groups, whereas *pomca* levels were significantly decreased in the HD and HD/HF groups compared to the LD group. *pomca* is expressed in the hypothalamus and the adenohypophysis (Forlano and Cone, 2007) and HD/HF-induced *pomca* reduction was even stronger in larvae from which the pituitary had been manually removed, revealing that it primarily reflects changes in hypothalamic *pomca* expression. Consistently, the expression of markers of defined second-order neurons downstream of Pomca and Agrp neurons was also reduced after excessive feeding (Figure 2A), such as thyroptropin-releasing hormone (*trh*) and oxytocin (*oxt*) (Kim et al., 2000; Sabatier et al., 2003). In contrast, studies in *pomca:EGFPras* transgenic reporter fish (see below for more details) revealed that HD and HD/HF feeding did not affect the number of Pomca neurons (Figure 2B), pointing to a specific effect on *pomca* transcription. Similar results were obtained when comparing age-matched LD, HD, and HD/HF larvae at 15 dpf (Figures S1D–S1M). At first sight, this negative regulation of *pomca* expression by food intake is a surprising finding for a satiety-signaling neuropeptide. However, this effect was only observed upon long-term overfeeding. In contrast, larvae exposed to a high-fat diet for only 6 hr displayed unaltered *gh1* and *agrp* expression levels but significantly increased *pomca* transcription (Figure 2C), in line with the response of *Pomc* to acute overfeeding in mammals.

Next, we aimed to investigate the mechanism underlying reduction of *pomca* transcription upon prolonged overfeeding. In mammals, transcription from the *Pomc* promoter is controlled by leptin and insulin signal transduction pathways (Varela and Horvath, 2012), while diet-induced obesity has been shown to cause severe but reversible leptin resistance of Pomc cells, characterized by low Pomc cell activation despite high leptin production by adipocytes (Enriori et al., 2007). Consistently, we found that in contrast to their LD controls, Pomca neurons of HD/HF zebrafish larvae failed to be activated upon treatment with human leptin as determined via phosphorylated version of extracellular signal-regulated kinase (pERK) immunofluorescence (IF) in the *pomca:EGFPras* transgenic line (Figures 2D–2I) (see below). In addition, juvenile zebrafish subjected to excessive feeding for 10 days displayed a much weaker induction (1.1-fold increase) of *pomca* transcription after intracerebroventricular (ICV) injection of human leptin than their respective normally fed controls (1.7-fold increase; Figure 2J).

Together, this indicates that reduced *pomca* expression in conjunction with elevated *gh1* expression is a specific consequence of long-term *ad libitum*/high-fat diet feeding, which is at least partly mediated by the evolutionary conserved occurrence of acquired leptin resistance.

Pomca Cells Do Not Project into the Adenohypophysis, and Pomca Innervation of the POA Is Not Altered upon Long-Term Overfeeding

In order to directly study Pomca neurons and their circuits in the context of somatic growth, we generated *pomca:EGFPras* (see also above) and *pomca:KalTA4* (attenuated Gal4VP16) transgenic zebrafish lines, which both fully recapitulate endogenous *pomca* expression (Figures S2A and S2B; data not shown). Pomca cell fibers built a complex network (Figure 3A), including innervations of the preoptic area (POA), the functional homolog of the rodent PVN (Herget et al., 2014; Peter, 1977), to where they send projections in very near proximity to *oxt*-, *trh*-, and *crh*-expressing cells (Figures 3E–3G). Notably, previous studies in zebrafish reported intense innervation of the pituitary by αMSH-positive axons (Zhang et al., 2012). However, in the *pomca:EGFPras* transgenic larvae, we only found few projections toward the pituitary. Most Pomca axons ran dorsal of the pituitary to cross the midline (Figures 3B–3D), or lateral of it (Figures 3C and 3D), and few axons entered the neurohypophysis (Figure 3C), while not a single projection was observed to directly target the adenohypophysis (Figures 3B–3D and S2C). Consistently, retrograde labeling of pituitary projections in *pomca:EGFPras* juveniles at 42 dpf failed to label hypothalamic Pomca neurons (Figure S2D), while IF analyses suggest that the former detection of hypophyseal axonal αMSH might have been caused by a cross-reactivity of the αMSH antibody with melanin-concentrating hormone (MCH) (Figures S2E–S2G).

In rodents, overnutrition during a critical time period of melanocortin system development is characterized by reduced Pomc cell projections to hypothalamic targets (Vogt et al., 2014). Instead, analysis of the Pomca cell circuitry in *pomca:EGFPras* transgenic zebrafish subjected to the long-term feeding paradigm revealed no detectable changes in POA innervation among the LD, HD, and HD/HF groups as assessed by quantification of axons innervating the POA or crossing the anterior commissure (Figures 3H–3L). Thus, distinct to rodents, overfeeding and/or application of a high-fat diet to zebrafish during stages of Pomca circuit development does not impair establishment of POA innervation. This may allow fish (in

(G–I) pERK and GFP levels in Pomca neurons of size-matched LD (G) and HD/HF (H) *pomca:EGFPras* larvae treated for 30 min with saline or leptin (n = 4 for each condition), and quantification of normalized values (I).

(J) Relative *pomca* mRNA levels in juveniles subjected to normal feeding (n = 8) or high-fat diet (HFD; n = 7) for 10 days, 4 hr after ICV injection of recombinant leptin, determined via qRT-PCR normalized against saline-injected controls.

Scale bars represent 50 μm (D) and 10 μm (E and F). a, $p < 0.05$; b, $p < 0.01$ relative to respective LD groups (A and C). Error bars in (A)–(C), (I), and (J) show SD.

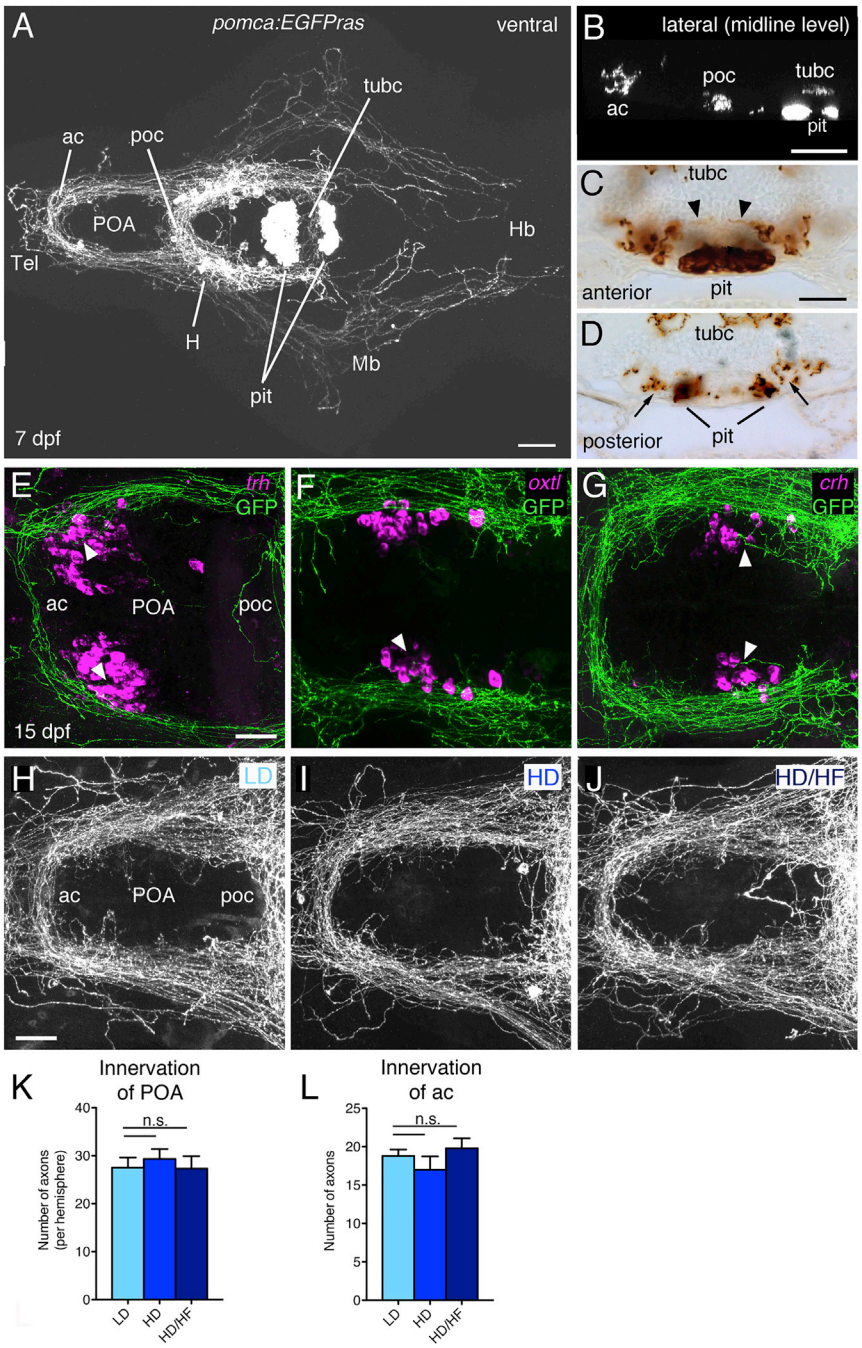

Figure 3. Analysis of Pomca Circuitry Reveals Sparse Pituitary Innervation by Pomca Axons and Unaltered POA Innervation after Excessive Feeding

(A–D) Anti-GFP IF (A and B) or immunohistochemistry (IHC) (C and D) on transgenic *pomca:EGFPras* larvae at 7 dpf.

(A) Cell bodies and projections of Pomca neurons in the hypothalamus (H) and *pomca*+ pituicytes (pit) in the adenohypophysis are labeled. Pomca neurons project to telencephalon (Tel), preoptic area (POA), midbrain (Mb), and hindbrain (Hb).

(B) Optical sagittal section at the level of the midline depicting Pomca axons crossing the anterior (ac), postoptic (poc), and the posterior tuberculum commissure (tubc) dorsal to the pituitary.

(C and D) Cross sections at anterior (C) and posterior (D) levels of the pituitary; Pomca axons are dorsal (arrowheads; entering neurohypophysis) or lateral (arrows) of the Pomca pituicytes of the adenohypophysis (pit).

(E–G) Fluorescent *in situ* hybridization (ISH) for *trh* (E), *oxt* (F), and *crh* (G) neurons in the POA (arrowheads) combined with anti-GFP IF in *pomca:EGFPras* larvae at 15 dpf.

(H–L) Unaltered POA innervation in *pomca:EGFPras* larvae subjected to LD (H), HD (I), or HD/HF (J) treatments, revealed by anti-GFP IF and subsequent quantification of axon number in the POA (K; n = 5) or anterior commissure (ac; L; n = 5).

Scale bars represent 100 μm (A and B), 50 μm (C and D), and 25 μm (E–J); n.s., not significant. Error bars in (K) and (L) show SD.

contrast to mammals) to better adapt to changes in environmental food availability.

Pomca Neurons Inhibit GH Expression

To investigate the function of Pomca neurons in the context of somatic growth, we used the nitroreductase (*nfsb*)/metronidazole (MTZ) system (Curado et al., 2008) to ablate hypothalamic and hypophyseal Pomca cells during late larval stages by treating *pomca:KalTA4*;*UAS:nfsb-Cherry* double transgenic fish with MTZ (Figures 4A and 4B). Pomca cell ablation resulted in a strong reduction of *pomca* transcript levels but a significant increase in *gh1* levels relative to non-ablated controls (Figure 4C). This effect can be fully attributed to the hypothalamic fraction of the Pomca cell population, as pituitary-specific ablation of Pomca cells with the *pomca*(pit):*CFP-nfsb* transgene still resulted in a reduction of *pomca* levels, whereas *gh1* expression levels remained unaffected (Figures 4D–4F). This negative effect of hypothalamic Pomca cells on *gh1* expression was further confirmed by pharmacological treatment of zebrafish larvae: incubation for 24 hr in medium containing 10 μM αMSH resulted in a significant reduction of *gh1* expression, whereas opposite effects were observed upon treatment with 10 μM of the Mc4r antagonist SHU9119 (Figure 4G). Collectively, this indicates that Pomca neurons inhibit *gh1* expression in an αMSH-dependent manner.

Pomca Cells Are Anatomically Connected to the Hypothalamo-Hypophyseal Somatotropic Axis

Neuroanatomical analyses in the *pomca:EGFPras* transgenics presented above clearly indicated that Pomca neurons do not

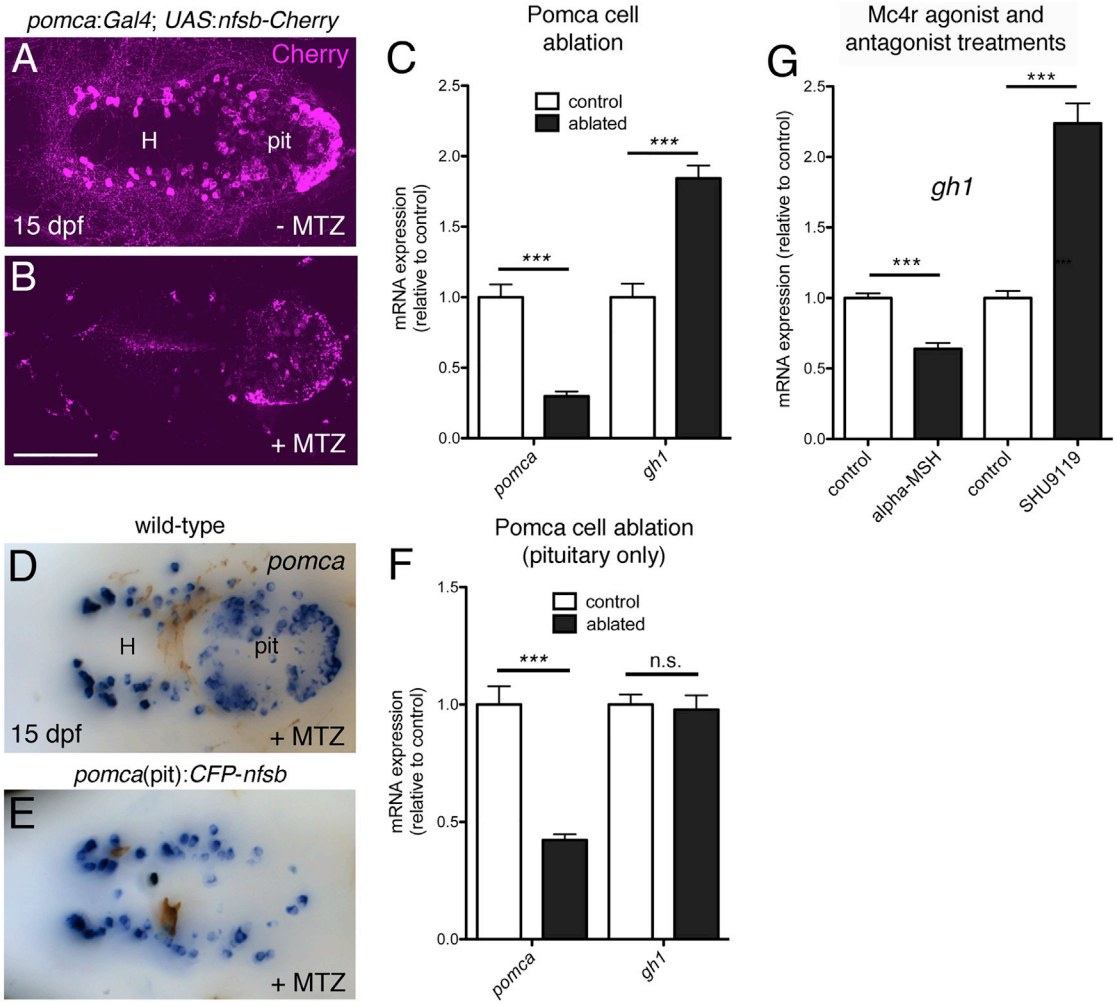

Figure 4. Pomca/αMSH Has a Negative Effect on *gh1* Expression

(A–C) Ablation of Pomca cells in hypothalamus and pituitary. Anti-RFP IF in *pomca:KalTA4*;*UAS:nfsb-Cherry* double transgenic larvae (15 dpf) without (A) or with MTZ treatment (B). (C) qRT-PCR analysis on *pomca:KalTA4* single transgenic larvae (control) compared to *pomca:KalTA4*;*UAS:nfsb-Cherry* double transgenic larvae (ablated) after 48-hr MTZ treatment revealing reduction of *pomca* (pointing to an ablation efficacy of ~75%) and elevation of *gh1* transcript levels.

(D–F) Pituitary specific ablation of Pomca cells. *pomca* ISH on MTZ-treated wild-type (D) and *pomca(pit):CFP-nfsb* transgenic (E) larvae at 15 dpf. (F) Selective loss of *pomca* in the pituitary results in decreased *pomca* levels but does not affect *gh1* expression as assessed by qRT-PCR. Abbreviations: pit, pituitary; H, hypothalamus.

(G) qRT-PCR analysis of *gh1* levels after treatment of 14 dpf zebrafish larvae with αMSH or SHU9119. Ventral views are shown in (A), (B), (D), and (E).

Scale bars represent 100 μm (A, B, D, and E); ***$p < 0.001$; n.s., not significant. Error bars in (C), (F), and (G) show SD.

directly project to the adenohypophysis but instead favor the possibility that second-order neurons are involved in mediating their negative effect on *gh1* expression and function. Sst-expressing hypothalamic neurons, well-characterized components of the somatotropic hypothalamo-hypophyseal axis, appeared as likely candidates, although so far have not been linked to the melanocortin circuitry, even in mammals. The zebrafish genome contains five different somatostatin genes, with *sst1.1* showing various expression domains, including the POA (Löhr et al., 2009). To analyze the projection patterns of zebrafish Sst1.1 neurons, we generated an *sst1.1:EGFPras* transgenic line (Figure 5A) that fully re-capitulates the endogenous sst1.1 expression (Figures S3A and S3B) and defines an anterior and posterior Sst1.1 cell domain within the POA (Figure 5D′). Strikingly, in contrast to Pomca cell projections (see above), the *gh1* domain of the larval adenohypophysis was intensely labeled by Sst1.1+ projections (Figure 5B). Retrograde labeling with DiI crystals placed into the pituitary of *sst1.1:EGFPras* juveniles (30 dpf) identified cells of the posterior POA cluster as the Sst1.1 neurons directly projecting to the adenohypophysis, whereas cells in the anterior POA domain or any other brain region did not reveal any co-label (Figures 5C–5D′; data not shown; n = 7/7).

In order to test whether such hypophysiotropic Sst1.1 cells can serve as direct targets for Pomca neurons and αMSH, we carried out *sst1.1 in situ* hybridization (ISH) and anti-GFP IF on *pomca:EGFPras* transgenics, revealing a clear pattern of innervation of the posterior Sst1.1 domain by Pomca cell axons

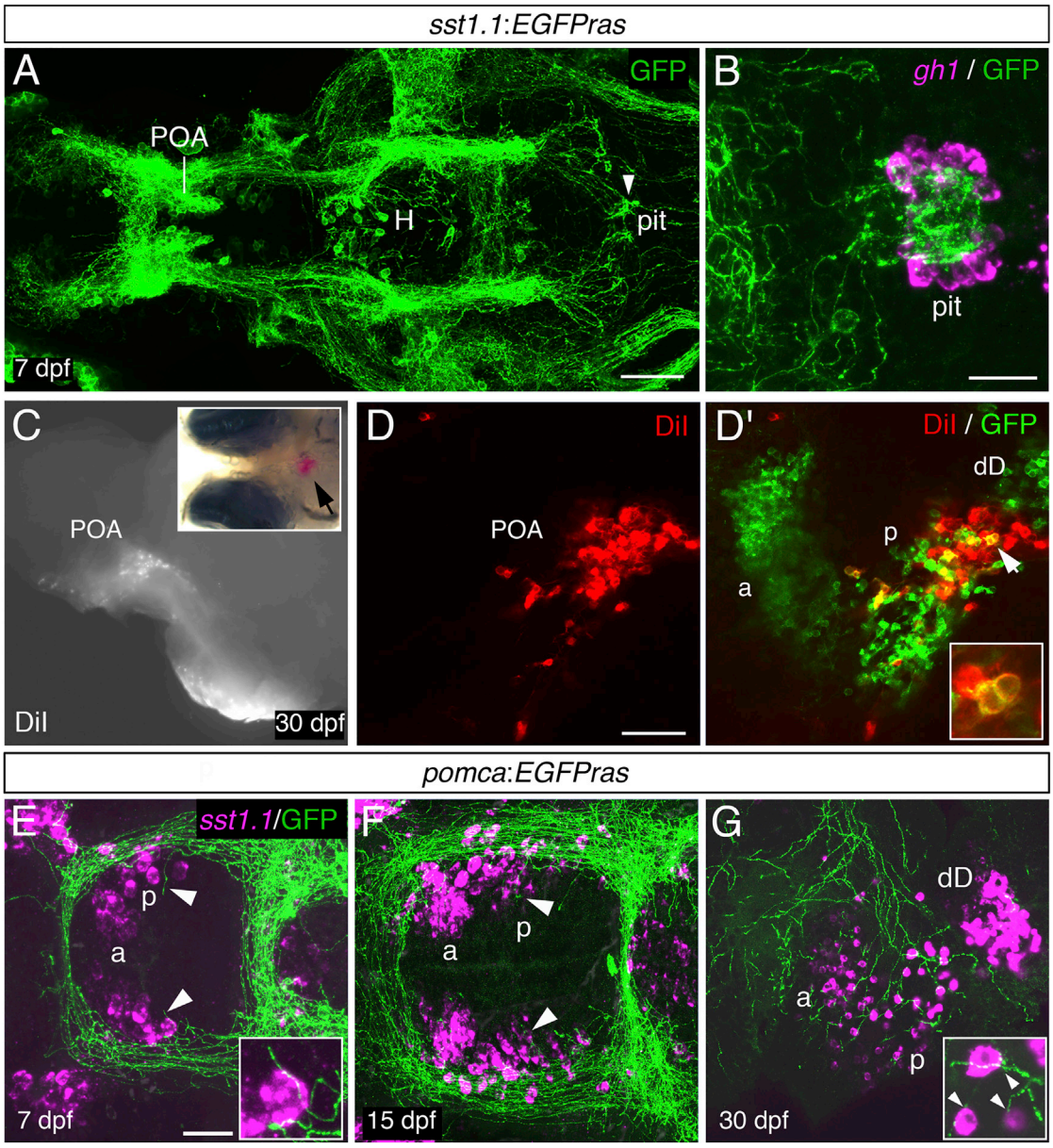

Figure 5. Sst1.1-Neurons of a Posterior POA Domain Project to Pituitary Somatotropes and Are Innervated by Pomca Cell Axons

(A) Anti-GFP IF on an *sst1.1:EGFPras* transgenic larva at 7 dpf. GFP+ axons innervating the pituitary (pit) are indicated by an arrowhead. H, hypothalamus; POA, preoptic area.

(B) *gh1* ISH (magenta) co-stained via anti-GFP IF (green) at 7 dpf reveals extensive innervation of the *gh1* domain in the adenohypophysis by GFP+ Sst1.1 axons.

(C–D′) Placement of DiI crystals into the pituitary of *sst1.1:EGFPras* fish at 30 dpf (C) retrogradely labels cell bodies in the POA (see arrowhead in inset for position of DiI). (D and D′) Within the POA, the posterior (p), but not the anterior (a) Sst1.1-cell domain, contains DiI+ cells. (D′, inset) Magnification of the region labeled by the arrowhead. Additional Sst1.1 cells (dD) are located outside the POA.

(E–G) *sst1.1* ISH combined with anti-GFP IF in *pomca:EGFPras* transgenic at 7 dpf (E), 15 dpf (F), and 30 dpf (G) showing innervation of the posterior Sst1.1 POA domain by Pomca-cell axons at all examined stages (see arrowheads and magnifications).

Scale bars represent 100 μm (A), 25 μm (B, E, and F), and 50 μm (D and G). Ventral views are shown in (A), (B), (E), and (F), and lateral views are shown in (C)–(D′) and (G).

(Figures 5E–5G) at all examined developmental stages. In addition, co-labeling *sst1.1:EGFPras* larvae via *mc4r* ISH and anti-GFP IF revealed broad expression of *mc4r* within the POA (Figures 6A–6A″), including hypophysiotropic Sst1.1+ cells of the posterior POA domain (Figures 6B-6B″). Together, this points to the presence of all neuroanatomical and structural prerequisites for a functional Pomca-Sst1.1-Gh1 hypothalamo-hypophyseal axis in the zebrafish brain. Strikingly, also in the mouse, 58.4% ± 10.2% of hypophysiotropic Sst cells of the PeVN/PVN (Figures 6C and 6C′) displayed Mc4r expression

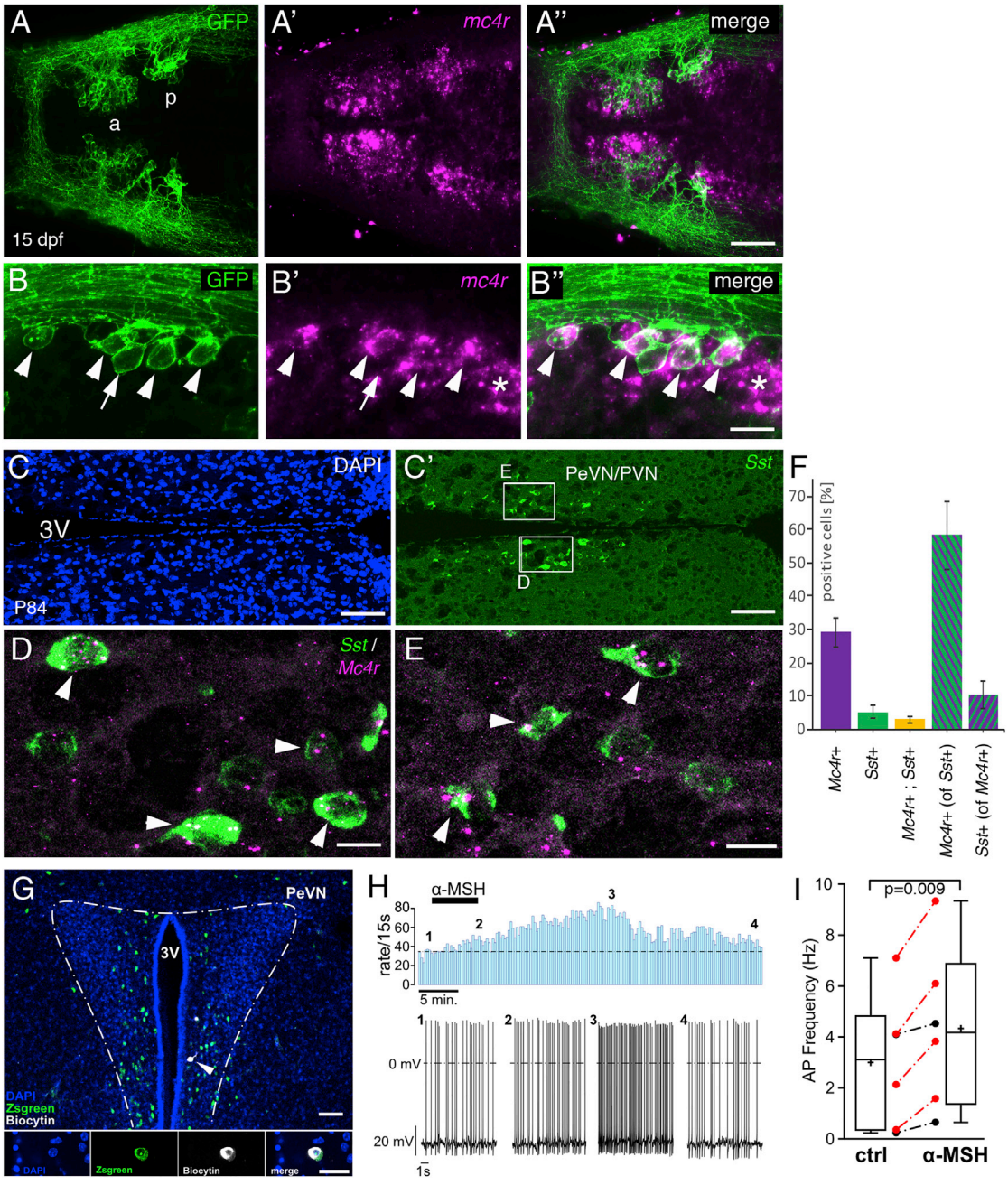

Figure 6. Hypophysiotropic Sst Neurons in Zebrafish and Mouse Express *mc4r* Transcript and Respond to αMSH in Mouse

(A–B′′) *sst1.1:EGFPras* transgenic zebrafish at 15 dpf, stained via anti-GFP IF (green; [A] and [B]) in combination with *mc4r* ISH (magenta; [A′] and [B′]). Merged images are shown in (A′′) and (B′′).

(A–A′′) Overview of the POA showing mc4r+ cells in Sst1.1+ neurons of anterior (a) and posterior (p) POA clusters.

(B–B′′) Magnification of the posterior POA domain revealing expression of *mc4r* by most GFP+ cells (arrowheads, mc4r+,sst1+; arrow, mc4r−,sst1+; asterisk, mc4r+,sst1−).

(C–E) ISH for *Sst* (green; [C′]–[E]) and *Mc4r* (red; [D] and [E]) on sections of P84 mouse brains, counterstained with DAPI (nuclei, blue; [C]).

(C and C′) Overview of the PeVN/PVN hypothalamic region containing hypopyhsiotropic Sst cells.

(D and E) Magnification of boxed areas in (C′). Mc4r+ Sst neurons are marked by arrowheads.

(F) Quantification of Mc4r+ and Sst+ cells relative to total cell number (DAPI+), and quantification of Mc4r+ cells relative to Sst+ cells and vice versa (in percentage). Error bars show SD.

Scale bars represent 50 μm (A′′), 25 μm (B′′), 100 μm (C and C′), and 15 μm (D and E).

(G–I) αMSH increases the activity of Sst neurons in the PeVN of SstZsGreen mice.

(legend continued on next page)

(Figures 6D–6F). In reverse, 10.3% ± 4.1% of Mc4r+ cells of the mouse PeVN/PVN displayed Sst expression, consistent with the formerly reported co-existence of Sst cells with multiple other potential αMSH target cells in this area (Biag et al., 2012) and similar to the incomplete overlap of *sst1.1* and *mc4r* expression in the zebrafish POA (Figures 6A–6B″). Together, this points to the evolutionary conservation of Pomc-Sst circuitry.

Functional Connection between αMSH, Sst1.1 Neurons and Somatostatin

We next set out to assess the functional impact of αMSH on hypophysiotropic Sst cells in fish and mouse. Perforated patch clamp recordings were performed in *Sst-IRES-Cre*;*R26-fl-rx⊿-ZsGreen* double transgenic mice (Experimental Procedures) from Sst PeVN neurons, which were pharmacologically isolated from GABAergic and glutamatergic input to minimize indirect modulatory effects. The neurons were identified by their position in the PeVN and by their fluorescent label (Figure 6G). 250 nM αMSH was bath-applied for 5–7 min, and the effect was measured 10 min after the onset of αMSH administration. In average, αMSH increased action potential frequency by ∼43% (from 3.0 ± 1.1 Hz to 4.3 ± 1.3 Hz; p = 0.009, n = 6). On the single-cell level, a significant increase in action potential frequency was observed in two-thirds of the recorded Sst neurons (Figure 6I), consistent with the obtained percentage of Sst neurons displaying Mc4r expression (Figure 6F). Of note, typically the stimulatory effect of αMSH continued to increase even further throughout the first ∼15 min of the washout and was not fully reverted even after a >30-min wash (Figure 6H), in line with the previously reported effects of αMSH on Mc4r+ PVN neurons (Ghamari-Langroudi et al., 2011).

To investigate the effect of αMSH on zebrafish Sst cells, we isolated the brains of *sst1.1:EGFPras* juveniles (42 dpf) and incubated one brain hemisphere in artificial cerebrospinal fluid (ACSF) and the other hemisphere in ACSF containing 10 μM αMSH. After incubation for 30 min, the αMSH-treated hemisphere displayed a strong increase of pERK levels, indicative of neuronal activation (Randlett et al., 2015), in hypophysiotropic Sst1.1 neurons of the posterior POA domain compared to the control hemisphere (Figures 7A–7G). Similar results were obtained upon ICV injection of 0.5 mg/kg αMSH into juvenile *sst1.1:EGFPras* fish at 42 dpf compared to saline-injected controls (Figures S2C and S2D). Furthermore, repetitive ICV injections of saline, 0.5 mg/kg αMSH, or 0.5 mg/kg SHU9119 over the course of 48 hr (saline: n = 17; αMSH: n = 11; SHU9119: n = 15) slightly increased or decreased *sst1.1* fluorescent ISH signal within the posterior POA domain 2 hr after the last αMSH or SHU9119 injection, respectively (Figure 7H). Finally, to test whether the effect of αMSH on somatic growth depends on somatostatin function, we carried out a pharmacogenetic epistasis analysis (Figure 7I). For this purpose, we treated zebrafish larvae at 14 dpf for 8 hr with 10 μM αMSH, 1 μM of the non-selective somatostatin receptor antagonist cyclo-somatostatin (cSST), or a combination of both and determined the effects on *gh1* transcript levels. αMSH treatment significantly reduced *gh1* expression compared to saline-treated controls, as reported above, while this effect was fully abrogated upon co-treatment with cSST.

Together, this indicates that the negative effect of αMSH on *gh1* transcription and somatic growth is mediated via somatostatin released by Sst1.1 neurons, which are direct targets of Pomca neurons and therefore hereby newly identified second-order neurons of the melanocortin system.

DISCUSSION

In the present study, we investigated the relationship between the melanocortin and somatotropic systems in zebrafish, an organism that displays a strong diet dependence of somatic growth (Leibold and Hammerschmidt, 2015). We identify a thus-far-unknown hypothalamo-hypophyseal αMSH/Pomca-somatostatin-GH axis promoting growth upon excessive food supply. Somatostatin-producing Sst1.1 neurons of the hypothalamic POA are a central part of this axis. These Sst1.1 cells are innervated by Pomca neurons, express the αMSH receptor Mc4r, and can be stimulated by exogenous αMSH. Thus, they fulfill all criteria to be regarded as second-order neurons of the melanocortin system, while in turn projecting to the pituitary to attenuate *gh1* expression. In accordance with such a net growth-inhibiting effect of Pomca/αMSH, ablation of Pomca neurons or treatment with an Mc4r antagonist led to increased, and treatment with αMSH to decreased *gh1* transcript levels. Strikingly, in co-treatment experiments, αMSH failed to attenuate *gh1* expression when endogenous somatostatin was inhibited, clearly indicating that its negative impact on growth is indirect and mediated in an Sst-dependent manner. These functional features are consistent with the structural equivalents of this circuitry as revealed through our transgenic reporter lines. In contrast, in a former report, the effect of the melanocortin system on *gh1* production had been attributed to direct αMSH and Agrp neuronal projections to the pituitary (Zhang et al., 2012), a mechanism that, according to our data, is of minor importance. However, the overall growth-promoting effect of Agrp reported by Zhang et al. (2012) is consistent with the growth-inhibiting effect of αMSH and Pomca neurons reported here.

A fundamental question remains: why do αMSH/Pomca neurons inhibit growth, given that they are normally active after feeding and when energy stores are filled, activated by

(G) Top: overview of the PeVN (300 μm brain slice) showing ZsGreen immunofluorescence (green) and the Sst neuron that was labeled with biocytin (white, arrow) during the recording (blue, DAPI). Bottom: higher-magnified view of a single optical section of recorded neuron's soma showing the DAPI−, Sst−, and biocytin label separately and merged (from left to right). Scale bars: overview, 50 μm; details, 20 μm. αMSH modulation of single Sst PeVN neuron (H). Firing rates (bin width 15 s) before, during, and after application of 250 nM αMSH (indicated by bar) (top). Original traces from the recording at indicated time points 1–4 (bottom). Boxplots showing the effect of αMSH (250 nM, 5–7 min) on the action potential frequency of Sst neurons measured 10 min after onset of αMSH application (p = 0.009, n = 6, from 5 mice; paired two-tailed t test) (I). Red symbols indicate neurons in which the increase in action potential frequency was larger than 3 × SD of the control, thus defining them as responsive. Whiskers indicate the minimum and maximum, and plus signs and horizontal lines indicate means and medians, respectively; error bars indicate SD.

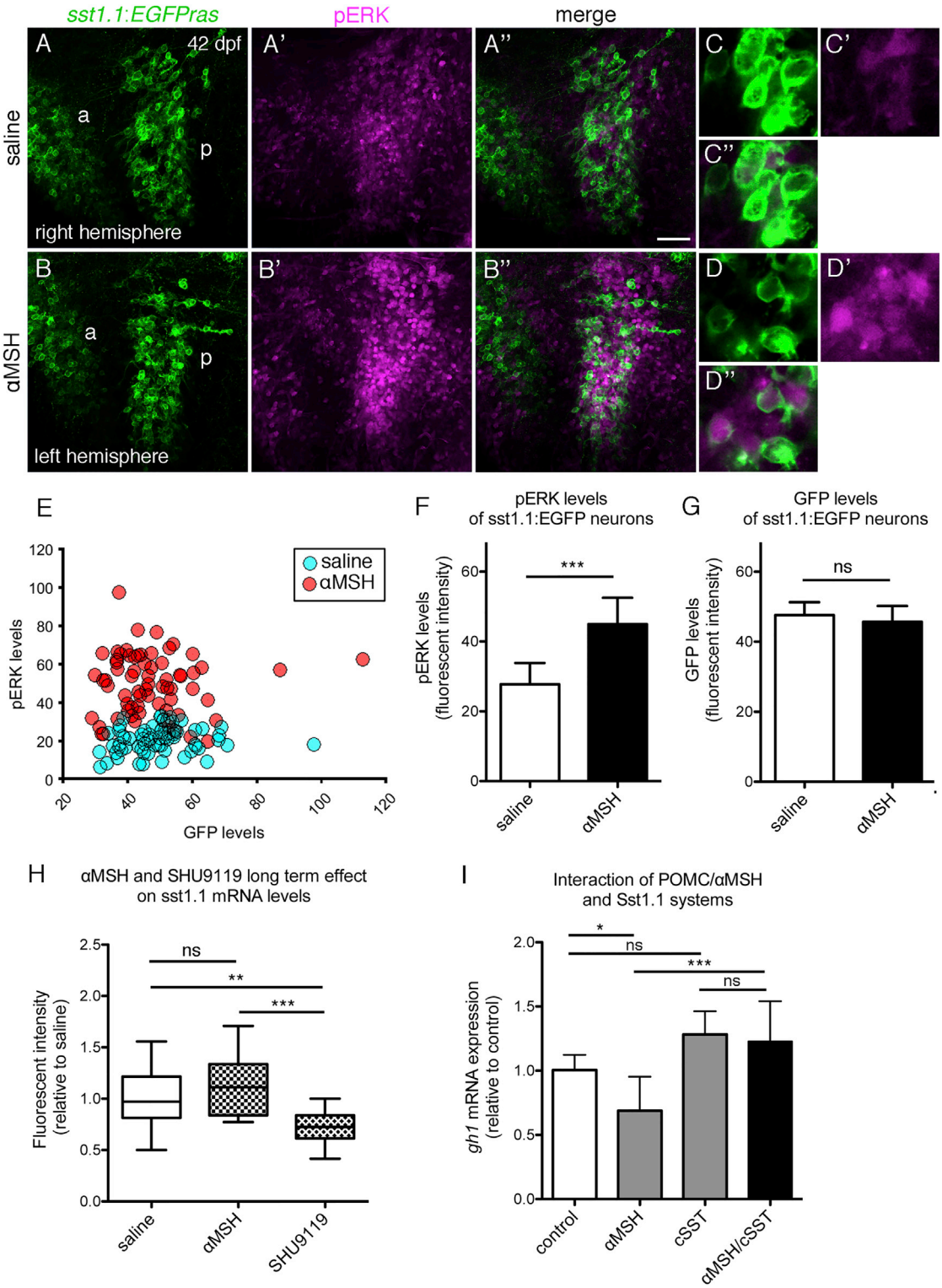

Figure 7. Zebrafish Sst Neurons Respond to αMSH to Mediate αMSH's Effect on GH Expression

(A–G) pERK response of hypophysiotropic Sst1.1 cells to αMSH treatment in *sst1.1:EGFPras* fish (42 dpf).

(A–B′′) POA of two hemispheres derived from the same brain, differentially incubated in saline (A–A′′) or 10 μM αMSH (B–B′′) for 30 min. Double IF for GFP (green) and pERK (magenta) reveals increase in pERK levels after αMSH application in the posterior POA (p). Images of the right hemisphere were flipped horizontally.

(C–D′′) Magnification of posterior POA Sst1.1 neurons without (C–C′′) or with (D–D′′) αMSH treatment.

(legend continued on next page)

energy-sensing signals like leptin to reduce appetite and promote energy expenditure? We recently showed that in zebrafish, somatic growth can be subordinate to other anabolic branches of energy expenditure, such as developmental pace in larvae and reproduction in adults (Leibold and Hammerschmidt, 2015). In this light, it makes sense in the short-term to attenuate *gh1* levels to reserve energy for biological processes other than growth and/or to reduce *gh1*-dependent lipolysis (McMenamin et al., 2013), thereby protecting lipid energy stores. In addition, such negative short-term effects might contribute to the circadian variations in GH secretion, which during wakeness (when food is taken up) is much lower than during sleep (Van Cauter et al., 1998).

Interestingly and most strikingly, however, we also found that this per se growth-inhibiting pathway can also be used to promote growth, when under conditions of long-term *ad libitum* feeding, *pomca* transcript levels do not rise, as only seen in short-term response to overfeeding, but even decline. This in turn results in decreased Sst1 neuron activation and a derepression of *gh1* expression. Thereby, it is ensured that upon continuously rich food resources, when energy prioritization is no longer required, larval zebrafish switch into a "seize-the-opportunity" mode, with reduced *pomca* levels allowing for unrestricted food intake and somatic growth. We could further show that this reduction in *pomca* transcription correlates with and might be caused by diet-induced leptin resistance of hypothalamic Pomca cells, similar to what has been reported for mammals (Enriori et al., 2007). However, leptin resistance was only demonstrated for exogenously supplied leptin, raising the possibility that our *ad libitum* fed fish are still capable of responding to endogenous leptin, similarly to what has been reported for diet-induced obese mice (Ottaway et al., 2015; Myers, 2015). Also, acquired leptin resistance per se can explain why *pomca* transcript levels in *ad-libitum*-fed fish are not higher, but not necessarily why they are even lower than in controls with restricted food supply. Therefore, it seems likely that other dietary factors in addition to diet-induced leptin resistance target the melanocortin system to regulate the activity of the somatotropic axis. However, all of these factors and mechanisms seem to interfere with the melanocortin system at the hormonal, rather than the anatomical level, as Pomca cell circuits' architecture remained unaltered in *ad-libitum*-fed fish. This is in contrast to findings in mouse where feeding high caloric diets to mothers during the lactation period impairs projections of both of POMC and Agrp neurons to various hypothalamic target nuclei (Vogt et al., 2014).

We have also obtained the first data suggesting that a Pomc-Sst-Gh axis is also active in mammals. GH transcription and release have long been known to be under negative control of Sst and positive control of Ghrh (Tauber and Rochiccioli, 1996). There was also indirect support for a functional correlation between Pomc and Sst, with obese/large Agouti-yellow mice displaying increased levels of the αMSH antagonist Agouti in combination with decreased Sst levels in the PeVN, whereas Ghrh levels are unaltered (Martin et al., 2006). However, whether mouse Sst neurons of the PeVN express Mc4R and respond to αMSH had not been elucidated before and is now shown here. Clearly, in contrast to fish, excessive food intake in mammals primarily promotes fat storage and obesity development, yet obese mammals also display a moderate increase in linear body size (Krude et al., 2003; Lu et al., 1994; Martinelli et al., 2011). Together, this suggests that a Pomc-Sst-Gh axis might also exist in mammals but might be less pronounced than in zebrafish or other teleosts with an even more advanced indeterminate growth. In addition, it appears that in conjunction with a strong Pomc-Sst-Gh axis, as in fish, diet-induced leptin resistance, possibly in cooperation with other diet-induced mechanisms, can elicit a favorable and possibly original function to promote unrestricted growth when food resources are rich, whereas in conjunction with a weaker axis, as in mammals, its adverse effects dominate, worsening obesity by attenuating the main negative feedback mechanism to burn energy and to restrict food uptake. Thus, leptin resistance may represent an evolutionary conserved concept that originated to sense long-term availability of rich fuel sources to allocate energy to somatic growth.

EXPERIMENTAL PROCEDURES

Zebrafish Lines and Mice Strains

The *Tg(pomca:EGFPras)*^{fr38Tg}, *Tg(pomca:KalTA4)*^{fr39Tg}, *Tg(sst1.1:EGFPras)*^{fr40Tg}, and *Tg(pomca(pit):CFP-nfsb;cmlc2:GFP)*^{fr41Tg} zebrafish lines were generated during the course of this study (Supplemental Experimental Procedures). The *Tg(UAS-E1b:nfsb-mCherry)*^{c264} line was previously described (Davison et al., 2007). All zebrafish experiments were approved by the national animal welfare committees (LANUV Nordrhein-Westfalen; 8.87-50.10.31.08.129; 84-02.04.2012.A251; 84-02.04.2012.A390; City of Cologne; 576.1.36.6.3.01.10 Be) and the University of Cologne. C57BL/6 mice were purchased from Charles River Laboratories, *Sst-IRES-Cre* mice (Taniguchi et al., 2011) from The Jackson laboratory (stock number 013044). For generation of *R26-fl-rxΔ-ZsGreen* transgenic and *Sst-IRES-Cre; R26-fl-rxΔ-ZsGreen* double transgenic mice, see Supplemental Experimental Procedures. Mice were housed under controlled environment in a 12h light/dark cycle, with food and water *ad libitum*. The procedures were approved by the Bezirksregierung (local authority in Cologne, Germany).

Larval Feeding Experiments

Starting at 5 dpf, 30 larvae per feeding group were transferred to plastic cylinders with a meshed bottom (9 cm diameter), each placed in a 1l beaker and filled with 200 mL of the appropriate paramecia suspension. Different concentrations of paramecia were obtained by directly feeding the stock culture (condition: high density [HD]), which corresponds to 400–500 paramecia per milliliter, or further diluting the stock 1:2 (condition: low density [LD]) in embryo medium. To generate high-caloric feeding conditions (HD/HF), larvae

(E–G) Quantification of pERK (E and F) and GFP (E and G) levels in a total of seven brain hemisphere pairs as shown in (A) and (B), revealing significantly increased pERK, but unaltered GFP levels in posterior Sst1.1 neurons after αMSH treatment.

(H) Effect of long-term αMSH or SHU9119 treatment on *sst1.1* mRNA levels. *sst1.1* FISH and signal intensity determination from confocal images of juvenile fish (42 dpf) that had been subjected to three repetitive ICV injections of αMSH, SHU9119, or saline over the course of 48 hr.

(I) Epistasis between Pomca/αMSH and Sst systems; *gh1* expression levels assessed by qRT-PCR analysis after treatment of larvae (14 dpf) for 8 hr with 10 μM αMSH, 1 μM cSST, or a combination of both peptides.

Scale bars represent 50 μm (A–B′) and 10 μm (C–D′). *$p < 0.05$; **$p < 0.01$; ***$p < 0.001$. Error bars in (F)–(I) show SD.

fed with concentrated paramecia stock were removed once per day from the cylinders and transferred to 50-mL tubes containing 30–40 mL 10% egg yolk (Proteinvital/Austria; 34% protein, 56% fat, and 4% carbohydrates) in embryo medium. Egg-yolk-treated larvae were incubated on a horizontal shaker for 6 hr and then returned to cylinders. Paramecia suspensions of all groups were exchanged once per day after egg yolk incubations. For acute egg yolk treatment, LD group larvae were incubated in 10% egg yolk for 6 hr at 14 dpf before sample collection.

Pharmacological Treatments

For pharmacological treatments of live zebrafish larvae, 6–8 specimen (14 dpf) per condition were incubated in 5 mL buffered embryo medium in a 6-well plate. Concentrations used were 10 μM αMSH (Sigma-Aldrich), 10 μM SHU9119 (Phoenix Pharmaceuticals), or 1 μM cSST (Tocris Bioscience). For controls, embryo medium without chemical additive was used. Incubation was performed in the dark at 28°C. αMSH and SHU9119 were applied for 24 hr. For the epistasis study (Figure 7I), αMSH, cSST, or a combination of both was applied for 8 hr. During chemical treatments, larvae did not receive food. After treatments, larvae were stored in Trizol until further processing.

For treatment with recombined human leptin (Figures 2D–2I), *pomca:EGFPras* transgenic larvae raised under LD or HD/HF conditions were sacrificed, the head was cut off, and the skull was opened/removed dorsally with fine forceps to allow diffusion of leptin into brain tissue. Heads were then incubated in ACSF (134 mM NaCl, 2.9 mM KCl, 2.1 mM $CaCl_2$, 1.2 mM $MgCl_2$, 10 mM glucose, and 10 mM HEPES, 290 mOsm, pH 7.8) with or without leptin (10 μM; Phoenix Pharmaceuticals) for 30 min at room temperature and fixed in 4% paraformaldehyde/PBS containing 0.25% TritonX.

For treatments of hemisphere explants (Figures 7A–7G), *Tg(sst1.1:EGFPras)*^{fr40Tg} juvenile fish (42 dpf) were sacrificed, brains were removed from the skull, and the two brain hemispheres were separated with a blade. For each brain, one hemisphere was incubated in 1 mL ACSF, and the other hemisphere was incubated in ACSF supplemented with 10 μM αMSH. After a 30-min incubation at room temperature, hemispheres were fixed in 4% paraformaldehyde/PBS containing 0.25% TritonX.

Cell Ablations

For global Pomca cell ablation, 15 double transgenic larvae (mCherry+) and 15 control siblings (mCherry−) from a cross of a *Tg(pomca:KalTA4)*^{fr39Tg} and a *Tg(UAS-E1b:nfsb-mCherry)*^{c264} transgenic fish were pre-sorted and collectively raised in one container to ensure identical feeding and raising conditions for both genotypes. For pituitary-specific Pomca cell expression, 15 transgenic larvae and 15 control siblings derived from a Tg(*pomca(pit):CFP-nfsb;cmlc2:GFP)*^{fr41Tg} outcross to a wild-type fish were raised in one container. Starting at 12 dpf, the larvae were treated with 7 mM Mtz (Sigma-Aldrich) for 48 hr followed by withdrawal of Mtz and a 18- to 20-hr recovery period. During treatment and recovery, larvae were supplied with food. The paramecia/Mtz suspension was exchanged once after 24-hr treatment. After ablation, *Tg(pomca:KalTA4)*^{fr39Tg}, *Tg(UAS-E1b:nfsb-mCherry)*^{c264} double transgenic larvae displayed well-visible remnants of mCherry signal in the pituitary and were separated from the controls at a fluorescent stereomicroscope. For *Tg(pomca(pit):CFP-nfsb;cmlc2:GFP)*^{fr41Tg} samples, the *cmlc2:GFP* reporter was used to separate transgenic from control larvae. All samples were stored in Trizol (Thermo Fisher Scientific) until used for further processing.

DiI Injections

Crystals of lipophilic carbocyanine dye (DiI; Thermo Fisher Scientific) were placed in the pituitary of *Tg(sst1.1:EGFPras)*^{fr40Tg} or *Tg(pomca:EGFPras)*^{fr38Tg} juvenile fish (30–42 dpf) using a microinjection setup. Briefly, fish were euthanized with tricaine and decapitated, and ventral head tissue was removed to expose the pituitary. After injection, the head was placed in 4% paraformaldehyde, and DiI was allowed to diffuse for 1 week at 4°C. After incubation, the brains were removed from the skull, washed with PBS, and directly imaged using a confocal microscope.

ICV Microinjections

Cerebroventricular microinjections were performed as previously described (Kizil and Brand, 2011). *Tg(sst1.1:EGFPras)*^{fr40Tg} juvenile fish (42 dpf) received 0.5 μg/g bodyweight αMSH or SHU9119 (injection volume, 500 nl) diluted in fish ACSF. Controls received ACSF only. For analysis of pERK activation (Figures S2C and S2D), fish received one injection of αMSH and were sacrificed 30 min post-injection, followed by fixation in 4% paraformaldehyde/PBS containing 0.25% TritonX. For evaluations of the long-term effects of αMSH and SHU9119 (Figure 7H), injections were performed twice a day during a 48-hr course. After each injection round, fish were connected to water circulation and food was supplied. 2 hr after the last injection, fish were sacrificed and brains were fixed in 4% paraformaldehyde/PBST (phosphate-buffered saline supplemented with 0.1% Tween 20). For leptin injections, wild-type juvenile fish were normally fed or excessively overfed (using carbohydrate- and lipid-rich dry food) from 42 to 51 dpf, followed by a single ICV injection of 1.0 μg/g bodyweight human leptin (Phoenix Pharmaceuticals) diluted in ACSF. Controls received ACSF only. Fish were euthanized 4 hr post-injection, and brains were removed and stored in Trizol (Figure 2J).

qRT-PCR

RNA from all samples was isolated using Trizol Reagent (Thermo Fisher Scientific) with the PureLink RNA Mini Kit (Thermo Fisher Scientific) including on-column DNaseI treatment followed by reverse transcription with Superscript II reverse transcriptase (Thermo Fisher Scientific). Gene expression was assayed by qPCR with SYBR Select Master Mix (Thermo Fisher Scientific) for *pparg*, *fabp11a*, *adipoqb*, *gh1*, *crh*, *trh*, *oxt*, *insa*, and normalized against ribosomal protein S23 transcript (*rps23*) (see Table S4 for primer sequences), or with TaqMan assays (Thermo Fisher Scientific) for *agrp*, *lepa*, *lepb*, and *pomca* also normalized against *rps23* (see Table S5 for assay IDs). qPCR was performed on an ABI-PRISM 7500 Fast Detection system. Fold differences were calculated using the $\Delta\Delta C_T$ method. For quantification of hypothalamus-specific *pomca* expression, the pituitary was removed from larvae using the *tg(pomca:EGFPras)*^{fr40Tg} line to control for complete removal.

Tissue-Labeling Procedures

Whole-mount fluorescent ISH (FISH), and whole-mount IF staining of zebrafish larvae were carried out as described in Supplemental Experimental Procedures. For Nile red staining of neural lipids, zebrafish larvae were incubated in a solution of 0.5 μg/ml Nile red (Sigma-Aldrich) for 10–15 min, carefully washed, and immediately subjected to imaging.

Detection of *Mc4r* and *Sst1* transcripts on mouse brain sections was carried out via RNAscope as described in the Supplemental Experimental Procedures.

Electrophysiology

Perforated patch-clamp experiments were performed on coronal brain slices (250–300 μm) from female and male $Sst^{ZsGreen}$ mice (6–9 weeks of age), which contained the PeVN. Experiments were carried out essentially as described previously (Hess et al., 2013; see Supplemental Experimental Procedures for details).

Statistics

All experiments were independently repeated at least three times. Results are presented in means ± SD. Statistical analyses were performed using Prism7 software (GraphPad Software). Tests for significance between groups were performed using an unpaired Student's t test or one-way ANOVA followed by a post hoc Tukey test. The significance threshold is $p < 0.05$.

SUPPLEMENTAL INFORMATION

Supplemental Information includes Supplemental Experimental Procedures, four figures, and six tables and can be found with this article online at https://doi.org/10.1016/j.celrep.2018.04.018.

ACKNOWLEDGMENTS

We thank the zebrafish community for sharing reagents and Gaurav Ahuja for help with DiI injections. Work in M.H.'s laboratory was supported by the German Research Foundation (DFG, CECAD, GRK 1960) and the National Institute of General Medical Sciences (GM63904).

AUTHOR CONTRIBUTIONS

H.L., S.L., C.S., and P.R. conceived, designed, performed, and analyzed the zebrafish experiments. M.M.A.P. designed and performed the mouse RNA scope experiments. S.H. carried out the electrophysiology studies. C.M.W. generated the R26-fl-rxΔ-ZsGreen mouse line. H.L., P.K., J.C.B., and M.H. conceived the project, designed the study, analyzed and interpreted data, and wrote the manuscript with input from all authors.

DECLARATION OF INTERESTS

The authors declare no competing interests.

Received: August 11, 2017
Revised: March 13, 2018
Accepted: April 2, 2018
Published: May 8, 2018

REFERENCES

Biag, J., Huang, Y., Gou, L., Hintiryan, H., Askarinam, A., Hahn, J.D., Toga, A.W., and Dong, H.W. (2012). Cyto- and chemoarchitecture of the hypothalamic paraventricular nucleus in the C57BL/6J male mouse: a study of immunostaining and multiple fluorescent tract tracing. J. Comp. Neurol. *520*, 6–33.

Cerdá-Reverter, J.M., Agulleiro, M.J., R, R.G., Sánchez, E., Ceinos, R., and Rotllant, J. (2011). Fish melanocortin system. Eur. J. Pharmacol. *660*, 53–60.

Chen, Y., Lin, Y.C., Kuo, T.W., and Knight, Z.A. (2015). Sensory detection of food rapidly modulates arcuate feeding circuits. Cell *160*, 829–841.

Curado, S., Stainier, D.Y., and Anderson, R.M. (2008). Nitroreductase-mediated cell/tissue ablation in zebrafish: a spatially and temporally controlled ablation method with applications in developmental and regeneration studies. Nat. Protoc. *3*, 948–954.

Davison, J.M., Akitake, C.M., Goll, M.G., Rhee, J.M., Gosse, N., Baier, H., Halpern, M.E., Leach, S.D., and Parsons, M.J. (2007). Transactivation from Gal4-VP16 transgenic insertions for tissue-specific cell labeling and ablation in zebrafish. Dev. Biol. *304*, 811–824.

Dhillo, W.S., Small, C.J., Seal, L.J., Kim, M.-S., Stanley, S.A., Murphy, K.G., Ghatei, M.A., and Bloom, S.R. (2002). The hypothalamic melanocortin system stimulates the hypothalamo-pituitary-adrenal axis in vitro and in vivo in male rats. Neuroendocrinology *75*, 209–216.

Eigler, T., and Ben-Shlomo, A. (2014). Somatostatin system: molecular mechanisms regulating anterior pituitary hormones. J. Mol. Endocrinol. *53*, R1–R19.

Enriori, P.J., Evans, A.E., Sinnayah, P., Jobst, E.E., Tonelli-Lemos, L., Billes, S.K., Glavas, M.M., Grayson, B.E., Perello, M., Nillni, E.A., et al. (2007). Diet-induced obesity causes severe but reversible leptin resistance in arcuate melanocortin neurons. Cell Metab. *5*, 181–194.

Farooqi, I.S., Yeo, G.S., Keogh, J.M., Aminian, S., Jebb, S.A., Butler, G., Cheetham, T., and O'Rahilly, S. (2000). Dominant and recessive inheritance of morbid obesity associated with melanocortin 4 receptor deficiency. J. Clin. Invest. *106*, 271–279.

Forlano, P.M., and Cone, R.D. (2007). Conserved neurochemical pathways involved in hypothalamic control of energy homeostasis. J. Comp. Neurol. *505*, 235–248.

Friedman, J. (2014). 20 years of leptin: leptin at 20: an overview. J. Endocrinol. *223*, T1–T8.

Friedman, J. (2016). The long road to leptin. J. Clin. Invest. *126*, 4727–4734.

Garfield, A.S., Shah, B.P., Burgess, C.R., Li, M.M., Li, C., Steger, J.S., Madara, J.C., Campbell, J.N., Kroeger, D., Scammell, T.E., et al. (2016). Dynamic GABAergic afferent modulation of AgRP neurons. Nat. Neurosci. *19*, 1628–1635.

Gesta, S., Tseng, Y.-H., and Kahn, C.R. (2007). Developmental origin of fat: tracking obesity to its source. Cell *131*, 242–256.

Ghamari-Langroudi, M., Srisai, D., and Cone, R.D. (2011). Multinodal regulation of the arcuate/paraventricular nucleus circuit by leptin. Proc. Natl. Acad. Sci. USA *108*, 355–360.

He, Q., and Karlberg, J. (2001). Bmi in childhood and its association with height gain, timing of puberty, and final height. Pediatr. Res. *49*, 244–251.

Herget, U., Wolf, A., Wullimann, M.F., and Ryu, S. (2014). Molecular neuroanatomy and chemoarchitecture of the neurosecretory preoptic-hypothalamic area in zebrafish larvae. J. Comp. Neurol. *522*, 1542–1564.

Hess, M.E., Hess, S., Meyer, K.D., Verhagen, L.A., Koch, L., Brönneke, H.S., Dietrich, M.O., Jordan, S.D., Saletore, Y., Elemento, O., et al. (2013). The fat mass and obesity associated gene (Fto) regulates activity of the dopaminergic midbrain circuitry. Nat. Neurosci. *16*, 1042–1048.

Huszar, D., Lynch, C.A., Fairchild-Huntress, V., Dunmore, J.H., Fang, Q., Berkemeier, L.R., Gu, W., Kesterson, R.A., Boston, B.A., Cone, R.D., et al. (1997). Targeted disruption of the melanocortin-4 receptor results in obesity in mice. Cell *88*, 131–141.

Imrie, D., and Sadler, K.C. (2010). White adipose tissue development in zebrafish is regulated by both developmental time and fish size. Dev. Dyn. *239*, 3013–3023.

Kim, M.S., Small, C.J., Stanley, S.A., Morgan, D.G., Seal, L.J., Kong, W.M., Edwards, C.M., Abusnana, S., Sunter, D., Ghatei, M.A., and Bloom, S.R. (2000). The central melanocortin system affects the hypothalamo-pituitary thyroid axis and may mediate the effect of leptin. J. Clin. Invest. *105*, 1005–1011.

King, C.M., and Hentges, S.T. (2011). Relative number and distribution of murine hypothalamic proopiomelanocortin neurons innervating distinct target sites. PLoS ONE *6*, e25864.

Kizil, C., and Brand, M. (2011). Cerebroventricular microinjection (CVMI) into adult zebrafish brain is an efficient misexpression method for forebrain ventricular cells. PLoS ONE *6*, e27395.

Krashes, M.J., Lowell, B.B., and Garfield, A.S. (2016). Melanocortin-4 receptor-regulated energy homeostasis. Nat. Neurosci. *19*, 206–219.

Krude, H., Biebermann, H., Schnabel, D., Tansek, M.Z., Theunissen, P., Mullis, P.E., and Grüters, A. (2003). Obesity due to proopiomelanocortin deficiency: three new cases and treatment trials with thyroid hormone and ACTH4-10. J. Clin. Endocrinol. Metab. *88*, 4633–4640.

Leibold, S., and Hammerschmidt, M. (2015). Long-term hyperphagia and caloric restriction caused by low- or high-density husbandry have differential effects on zebrafish postembryonic development, somatic growth, fat accumulation and reproduction. PLoS ONE *10*, e0120776.

Löhr, H., Ryu, S., and Driever, W. (2009). Zebrafish diencephalic A11-related dopaminergic neurons share a conserved transcriptional network with neuroendocrine cell lineages. Development *136*, 1007–1017.

Lu, D., Willard, D., Patel, I.R., Kadwell, S., Overton, L., Kost, T., Luther, M., Chen, W., Woychik, R.P., Wilkison, W.O., et al. (1994). Agouti protein is an antagonist of the melanocyte-stimulating-hormone receptor. Nature *371*, 799–802.

Martin, N.M., Houston, P.A., Patterson, M., Sajedi, A., Carmignac, D.F., Ghatei, M.A., Bloom, S.R., and Small, C.J. (2006). Abnormalities of the somatotrophic axis in the obese agouti mouse. Int. J. Obes. *30*, 430–438.

Martinelli, C.E., Keogh, J.M., Greenfield, J.R., Henning, E., van der Klaauw, A.A., Blackwood, A., O'Rahilly, S., Roelfsema, F., Camacho-Hübner, C., Pijl, H., and Farooqi, I.S. (2011). Obesity due to melanocortin 4 receptor (MC4R) deficiency is associated with increased linear growth and final height, fasting hyperinsulinemia, and incompletely suppressed growth hormone secretion. J. Clin. Endocrinol. Metab. *96*, E181–E188.

McMenamin, S.K., Minchin, J.E.N., Gordon, T.N., Rawls, J.F., and Parichy, D.M. (2013). Dwarfism and increased adiposity in the gh1 mutant zebrafish vizzini. Endocrinology *154*, 1476–1487.

Myers, M.G., Jr. (2015). Leptin keeps working, even in obesity. Cell Metab. *21*, 791–792.

O'Rahilly, S. (2014). 20 years of leptin: what we know and what the future holds. J. Endocrinol. *223*, E1–E3.

Ottaway, N., Mahbod, P., Rivero, B., Norman, L.A., Gertler, A., D'Alessio, D.A., and Perez-Tilve, D. (2015). Diet-induced obese mice retain endogenous leptin action. Cell Metab. *21*, 877–882.

Parichy, D.M., Elizondo, M.R., Mills, M.G., Gordon, T.N., and Engeszer, R.E. (2009). Normal table of postembryonic zebrafish development: staging by externally visible anatomy of the living fish. Dev. Dyn. *238*, 2975–3015.

Peter, R.E. (1977). The preoptic nucleus in fishes: a comparative discussion of function-activity relationships. Am. Zool. *17*, 775–785.

Randlett, O., Wee, C.L., Naumann, E.A., Nnaemeka, O., Schoppik, D., Fitzgerald, J.E., Portugues, R., Lacoste, A.M., Riegler, C., Engert, F., and Schier, A.F. (2015). Whole-brain activity mapping onto a zebrafish brain atlas. Nat. Methods *12*, 1039–1046.

Sabatier, N., Caquineau, C., Dayanithi, G., Bull, P., Douglas, A.J., Guan, X.M.M., Jiang, M., Van der Ploeg, L., and Leng, G. (2003). Alpha-melanocyte-stimulating hormone stimulates oxytocin release from the dendrites of hypothalamic neurons while inhibiting oxytocin release from their terminals in the neurohypophysis. J. Neurosci. *23*, 10351–10358.

Savastano, S., Di Somma, C., Barrea, L., and Colao, A. (2014). The complex relationship between obesity and the somatropic axis: the long and winding road. Growth Horm. IGF Res. *24*, 221–226.

Song, Y., and Cone, R.D. (2007). Creation of a genetic model of obesity in a teleost. FASEB J. *21*, 2042–2049.

Taniguchi, H., He, M., Wu, P., Kim, S., Paik, R., Sugino, K., Kvitsiani, D., Fu, Y., Lu, J., Lin, Y., et al. (2011). A resource of Cre driver lines for genetic targeting of GABAergic neurons in cerebral cortex. Neuron *71*, 995–1013.

Tauber, M., and Rochiccioli, P. (1996). Exploration of the somatotropic axis. Diabetes Metab. *22*, 240–244.

Timper, K., and Brüning, J.C. (2017). Hypothalamic circuits regulating appetite and energy homeostasis: pathways to obesity. Dis. Model. Mech. *10*, 679–689.

Van Cauter, E., Plat, L., and Copinschi, G. (1998). Interrelations between sleep and the somatotropic axis. Sleep *21*, 553–566.

Varela, L., and Horvath, T.L. (2012). Leptin and insulin pathways in POMC and AgRP neurons that modulate energy balance and glucose homeostasis. EMBO Rep. *13*, 1079–1086.

Vogt, M.C., Paeger, L., Hess, S., Steculorum, S.M., Awazawa, M., Hampel, B., Neupert, S., Nicholls, H.T., Mauer, J., Hausen, A.C., et al. (2014). Neonatal insulin action impairs hypothalamic neurocircuit formation in response to maternal high-fat feeding. Cell *156*, 495–509.

Wang, D., He, X., Zhao, Z., Feng, Q., Lin, R., Sun, Y., Ding, T., Xu, F., Luo, M., and Zhan, C. (2015). Whole-brain mapping of the direct inputs and axonal projections of POMC and AgRP neurons. Front. Neuroanat. *9*, 40.

Yaswen, L., Diehl, N., Brennan, M.B., and Hochgeschwender, U. (1999). Obesity in the mouse model of pro-opiomelanocortin deficiency responds to peripheral melanocortin. Nat. Med. *5*, 1066–1070.

Zhang, Y., Proenca, R., Maffei, M., Barone, M., Leopold, L., and Friedman, J.M. (1994). Positional cloning of the mouse obese gene and its human homologue. Nature *372*, 425–432.

Zhang, C., Forlano, P.M., and Cone, R.D. (2012). AgRP and POMC neurons are hypophysiotropic and coordinately regulate multiple endocrine axes in a larval teleost. Cell Metab. *15*, 256–264.

Cell Reports, Volume *23*

Supplemental Information

Diet-Induced Growth Is Regulated via Acquired Leptin Resistance and Engages a Pomc-Somatostatin-Growth Hormone Circuit

Heiko Löhr, Simon Hess, Mafalda M.A. Pereira, Philip Reinoß, Sandra Leibold, Christel Schenkel, Claudia M. Wunderlich, Peter Kloppenburg, Jens C. Brüning, and Matthias Hammerschmidt

Supplemental Figures

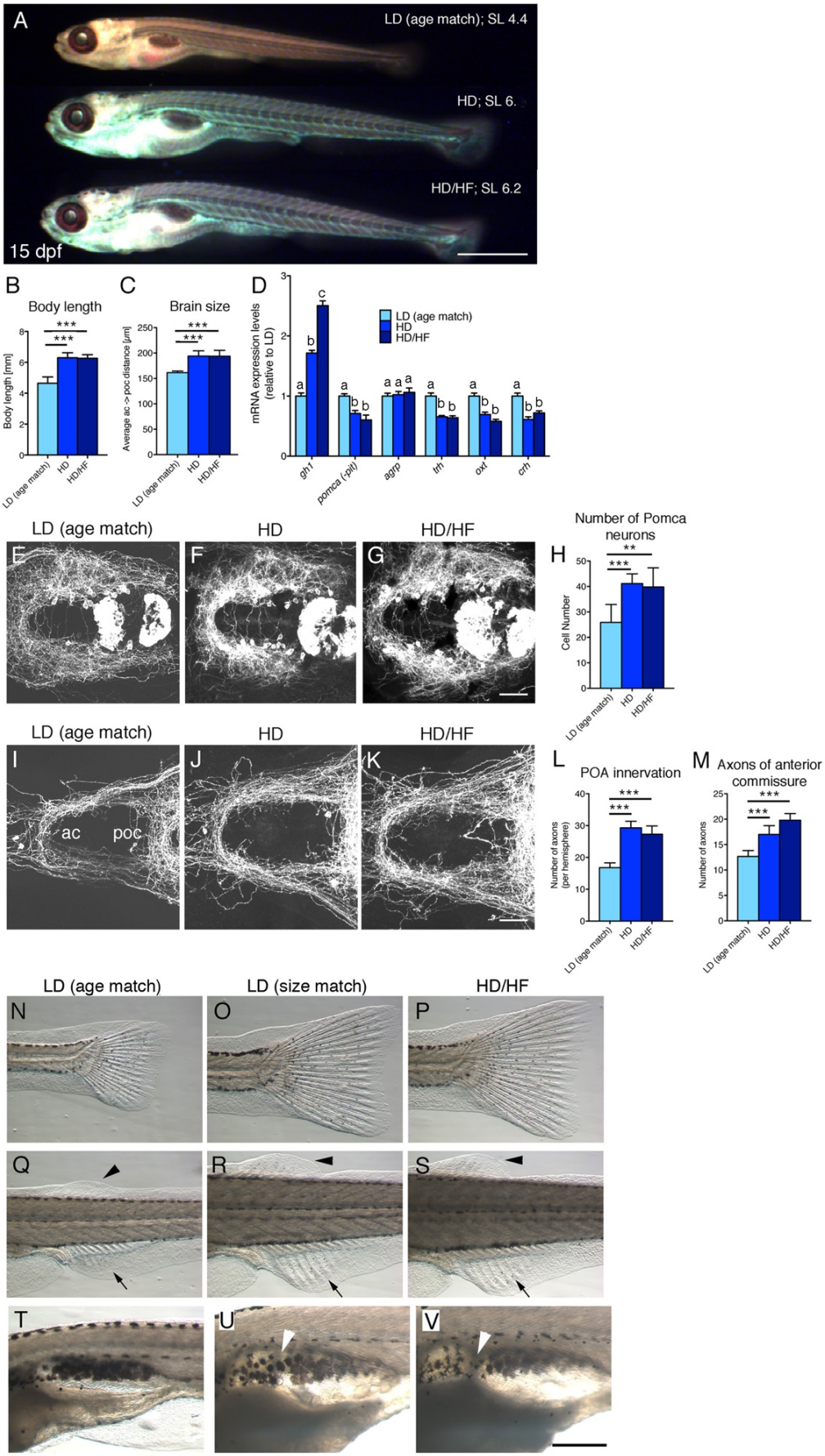

Figure S1: Strong impact of caloric input on somatic growth, neuronal circuit formation and developmental pace of zebrafish larvae – comparisons between age-matched larvae. Related to Figures 1 and 2.

Effects of caloric input on zebrafish larvae raised under LD, HD, or HD/HF feeding conditions from 5 -15 dpf. Analyses were performed at 15 dpf for all groups (age matched). (A) Lateral overview of larvae at 15 dpf stained with Nile red revealing strong differences in body length between LD (age match; standard body length (SL) = 4.4 mm) and HD (standard body length = 6.0 mm), HD/HF larvae (standard body length = 6.2 mm), respectively. Also note differences in fluorescent color profiles of Nile red likely reflecting differences in body fat composition. (B) Quantifications of body length (n=50) and (C) distance between anterior and postoptic commissures as a measure for brain size in *pomca:EGFPras* transgenic fish (n=5). (D) qRT-PCR analyses: mRNA levels for *gh1*, *pomca* (only neuronal fraction), *agrp*, *trh*, *oxt* and *crh*. Columns with different superscript letters (a,b,c) are significantly different from each other ($p<0.05$) according to ANOVA followed by a post hoc Tukey test. (E-M) Reduced number of Pomca hypothalamic neurons (E-H) and reduced innervation of preoptic area (POA) and anterior commissure (ac) in LD (age match) larvae compared to HD and HD/HF larvae assessed by anti-GFP IF on *pomca:EGFPras* transgenics (E-G; I-K) and subsequent quantifications of cell (H; n = 10) and axon numbers (L-M; n = 10). (N-V) Evaluation of developmental progress using anatomical criteria according to Parichy et al. (2009) revealing slower postembryonic development of LD (age match) larvae compared to HD and HD/HF larvae. (N-S) Development of caudal (N-P), dorsal (arrowhead in Q-S) and anal fins (arrow in Q-S) showing differences between LD (age match) versus HD and HD/HF larvae. (T-V) Budding of the anterior lobe of the swimbladder (arrowheads in T-V) has already taken place in HD and HD/HF but not in LD (age match) larvae. Scale bars: (A) 1 mm; (G) 50 µm for (E-G); (K) 50 µm for (I-K); (V) 250 µm for (N-V). p-values: (B, C, H, L, M) ** $p < 0.05$; *** $p < 0.01$ relative to LD (age match). Error bars in (B, C, D, H, L, M) show SD. (A, N-V) lateral views; (E-G; I-K) ventral views.

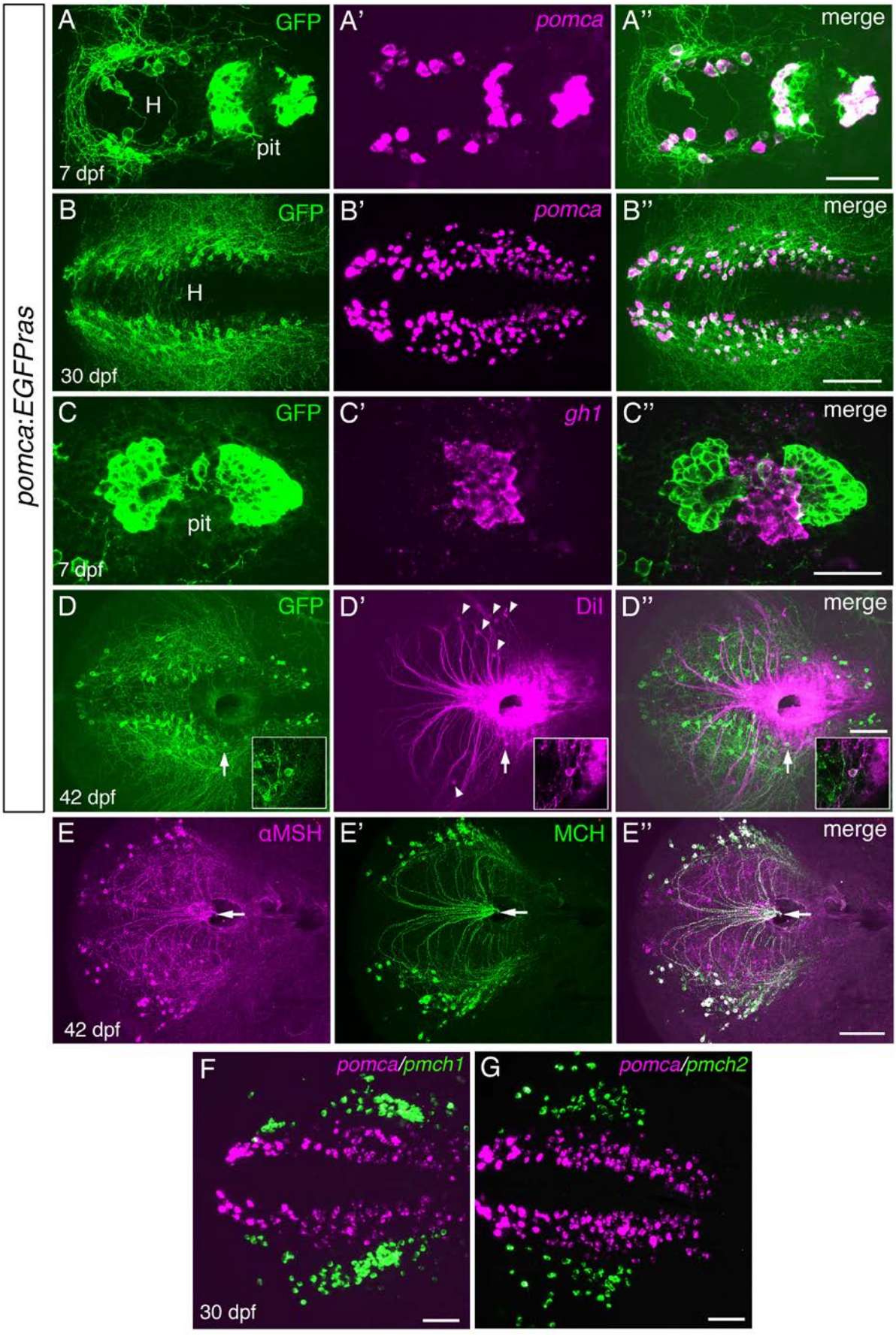
pomca:EGFPras
A
GFP
H
pit
7 dpf
A'
pomca
A''
merge
B
GFP
H
30 dpf
B'
pomca
B''
merge
C
GFP
pit
7 dpf
C'
gh1
C''
merge
D
GFP
42 dpf
D'
DiI
D''
merge
E
αMSH
42 dpf
E'
MCH
E''
merge
F
pomca/pmch1
30 dpf
G
pomca/pmch2

Figure S2. *pomca*:*EGFPras* transgenic zebrafish recapitulate endogenous *pomca* expression and reveal absence of adenohypophyseal innervation. Related to Figure 3.

(A-D'') *pomca*:*EGFPras* transgenic line. (A-B'') Fluorescent *in situ* hybridization (FISH) for *pomca* (magenta) followed by anti-GFP immunofluorescence (IF; green). All Pomca cells in hypothalamus (H) and pituitary (pit) are GFP+ at 7dpf. (B-B'') Co-localization of *pomca* transcripts and GFP in the hypothalamus at 30 dpf. (C-C'') FISH for *gh1* (magenta) and GFP IF (green) at 7 dpf revealing absence of Pomca cell-derived axons in regions of somatotropic cells of the pituitary. (D-D'') DiI injection into the pituitary at 42 dpf labels various hypothalamic neurons lateral to the Pomca cell domain (arrowheads). In three analyzed brains, only one single Pomca neuron (GFP+; arrow) was found to be co-labeled with DiI tracer (see D-D'' insets with magnified views). (E-E'') Co-IF for αMSH and MCH at 42 dpf reveals cross-reactivity of the anti-αMSH antibody with MCH peptide. All projections towards the pituitary (arrows) are double-positive and thus derived from MCH neurons. (F-G) Double FISH for *pmch1* (E, magneta) or *pmch2*, (F, magneta) and *pomca* (green) in wild-type brains at 30 dpf. Both *pmch1* and *pmch2* expressing cells are located lateral to the Pomca cell domain, most likely corresponding to the αMSH+ but GFP- cell bodies in (E). Scale bars: (A'') 50 µm, (B'') 100 µm, (C'') 50 µm, (D'', E'', F, G) 100 µm.

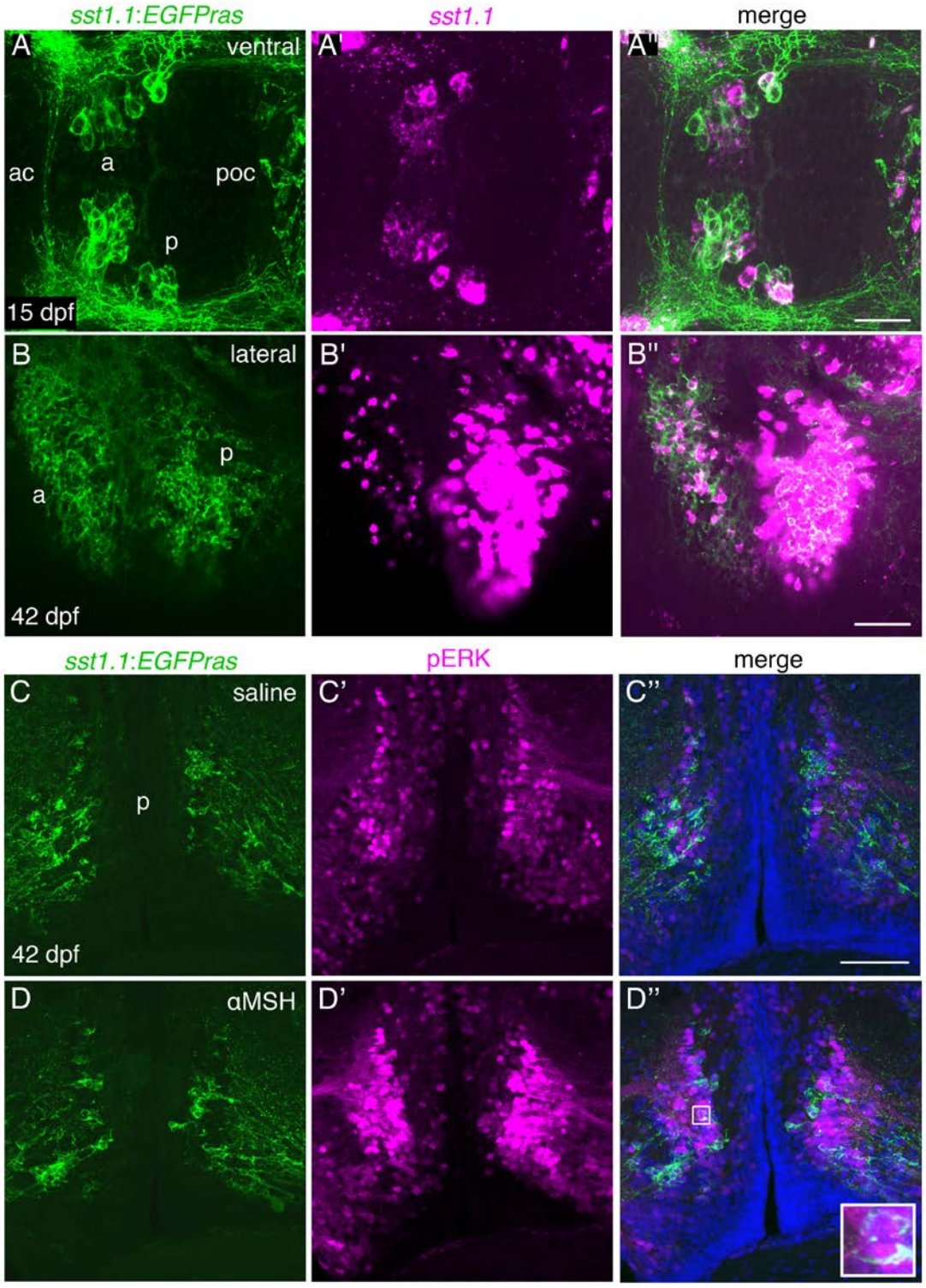

Figure S3. The *sst1.1:EGFPras* transgenic line recapitulates endogenous *sst1.1* expression and reveals activation of hypophysiotropic Sst1.1 neurons after αMSH ICV injection. Related to Figures 5 and 7.

(A-B'') *sst1.1* FISH (magenta) in combination with GFP IF (green) in *sst1.1:EGFPras* transgenic fish at 15 dpf (A-A'') and 42 dpf (B-B'') revealing co-localization of *sst1.1* transcripts and GFP both in the anterior (a) and posterior (p) domains of the preoptic

area (POA). (C-D'') Co-IF for GFP (green) and pERK (magenta) on cross-sections (12 µm) at the level of posterior Sst1.1 POA cell clusters of *tg(sst1.1:EGFPras)* fish (42 dpf), 30 min after cerebroventricular injection of saline (C-C'') or αMSH/saline (D-D''). pERK levels are strongly increased after αMSH application in a broad region of the POA including Sst1.1 neurons (see arrowheads and inset in D''). Scale bars: (A''): 50 µm, (B'', C'') 100 µm. ac: anterior commissure, poc, postoptic commissure.

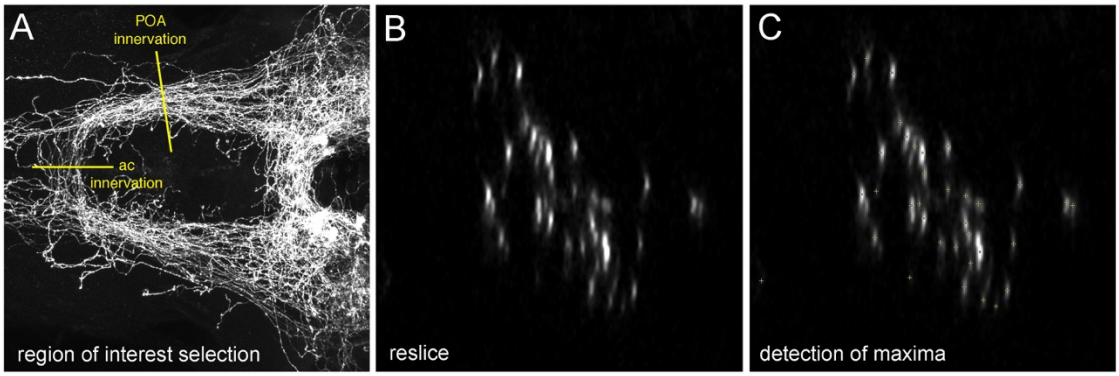

Figure S4. Automated quantification of axon numbers in larval zebrafish brains. Related to Experimental Procedures.

(A-C) Anti-GFP IF on a *Tg(pomca:EGFPras)*^{fr38Tg} larvae at 14 dpf. (A) Confocal image series (z-series) of the preoptic area (POA). Yellow lines depict regions of interest for quantification of axonal innervation of the POA or anterior commissure (ac), respectively. (B) Generation of optical cross sections using the „Reslice“ tool, from Fiji Software (Image J, NIH) allows for visualization of single axons in the respective area. (C) Automated quantification of axons using the „Find Maxima“ function of Fiji Software. Quantified spots are indicated by yellow crosses.

Supplemental Tables

Table S1. Primers used for BAC recombination. Related to Experimental Procedures.

Name	**Sequence (5'-3')**
pomca-hom-F-EGFP	ACAATATGAATTTAACATGCTTAAATGTGAATTGTATTGTGTTC TCAGAGaccatggtgagcaagggcgaggag
pomca-hom-F-mCherry	ACAATATGAATTTAACATGCTTAAATGTGAATTGTATTGTGTTC TCAGAGgccgccaccatggtgagcaagggcgaggaggac
pomca-hom-F-KalTA4	ACAATATGAATTTAACATGCTTAAATGTGAATTGTATTGTGTTC TCAGAGgccgccaccatgaaactgctctcatccatc
pomca-hom-R-KanR	TTTCCCAACACTGAGCTCTGACTTCAGATCCTCCTGCGCAGA GAACAGCCggactagtctattccagaagtagtgaggag
pTarbac2.1_iTol2-hom-F	GTCGACGGCCAGGCGGCCGCCAGGCCTACCCACTAGTCAAT TCGGGAGGAC*cctgctcgagccgggcccaagtg*
pTarbac2.1_iTol2-hom-R	GTTCATGTCTCCTTCTGTATGTACTGTTTTTTGCGATCTGCCG TTTCGA*attatgatcctctagatcagatct*
sst1.1-hom-F-EGFP	ACGCATCTCTCTTCTTTTACTCTGAGACCAAATAAACACTTTA ATAAAAGaccatggtgagcaagggcgaggag
sst1.1-hom-R-KanR	GCTGACGGCGAGCGCGAGGGACAGGAGCGCCAGTGCGCAC TGGATACGCGggactagtctattccagaagtagtgaggag
pIndigoBAC_iTol2-hom-F	GGTGCCTAATGAGTGAGCTAACTCACATTAATTGCGTTGCGC TCACTGCCC*cctgctcgagccgggcccaagtg*
pIndigoBAC_iTol2-hom-R	GGCCGATTCATTAATGCAGCTGGCACGACAGGTTTCCCGACT GGAAAGCG*attatgatcctctagatcagatct*

(upper case letters: BAC homology arms; lower case letters: cassette specific sequences)

Table S2. Primers used for gateway cloning. Related to Experimental Procedures.

Name	**Sequence (5'-3')**
pomca(pit)5'_attB4	**GGGG ACA ACT TTG TAT AGA AAA GTT G**GA GCT CCT ATC AAA CCA TGT T
pomca(pit)5'_attB1r	**GGGG AC TGC TTT TTT GTA CAA ACT TG**C CTC TGA GAA CAC AAT ACA ATT CAC
CFP-nfsb -attB1	**GGGG ACA AGT TTG TAC AAA AAA GCA GGC T**CC GCC ACC ATGGTGAGCAAGGGCGAGGAGCTGT
CFP-nfsb-attB2	**GGGG AC CAC TTT GTA CAA GAA AGC TGG GT**A TTACACTTCGGTTAAGGTGATGTT

(bold letters: att sites; normal letters: cassette specific sequences)

Table S3. Primers used for generation of R26-fl-rxΔ-ZsGreen mice. Related to Experimental Procedures.

Name	Sequence (5'-3')
5Asc2a ZsGreen	GGCGCGCCACCATGGGTTTAAACCGCGCGGAAGGCCGCGGCAG CCTGCTGACCTGCGGCGATGTGGAAGAAAACCCAGGGCCGGGC AAGAAGAAGAGGAAGGTGGCCCAGTCC AAGCACGGCCTGACCA
3Sma ZsGreen	CCCGGGATTTAAATTCAGGGCAAGGCGGA
5Mlu roxwss	ACGCGTTAACTTTAAATAATTGGCATTATTTAAAGTTACTCGAG GGATCTTTGTGAAG
3Asc roxwss	GGCGCGCCTAACTTTAAATAATGCCAATTATTTAAAGTTAAAGC TTACTTACCATGTCAG

Table S4. SYBR-Green qPCR primer sequences. Related to Experimental Procedures.

Gene	Sequence F (5'-3')	Sequence R (5'-3')
pparg	TGCCGCATACACAAGAAGAG	ATGTGGTTCACGTCACTGGA
fabp11a	GGCAAACTTGTGCAGAAACA	GAACTGAGCCTGGCATCTTC
adipoqb	ACAAGAACGACAAGGCCATC	AAAACCGGAGAAGGTGGAGT
rps23	TGTGCTTGAGAAAGTTGGTGTTG	AGCTGGACTCTCACACACTTCCT
trh	CGCTCCATCCTCACACAGAT	CTGTCGCTTCTCCATCCACT
insa	CCACCACCATATCCACCATT	ACCAACAGGACCAACAGAGC
gh1	GGTGGTTAGTTTGCTGGTGAA	CGTCTCGATGGAGTCAGAGTT
oxt	AACGCTCTGTTCAGGACTGG	AGGGAGAAAATCCTCCTCCA
crh	GCGCAAAGTTCAAAAACCAT	GCTGCTCTCGATGGCTCTAC

Table S5. TaqMan gene expression assays. Related to Experimental Procedures.

Gene	Specifications
pomca	commercially available Assay ID: Dr03112624_m1
rps23	commercially available Assay ID: Dr03430371_m1
agrp	custom made F: ATCATCTGCCCTGCTGCAA R: GCCTTAAAGAAGCGGCAGTAG Probe: CCCCTGCGACACCTG
lepa	custom made F: CATCGTCAGAATCAGGGAACACA R: GTCCTGGATCCCCAATGATGAG Probe: TTGACGGGCAAAATT
lepb	custom made F: GAACCACCATCAGCCGAATTAAAA R: GCCGAAATCAATCTCTGGAGACAT Probe: CTGGAAGTGCTCATCTTT

Table S6. Primary antibodies. Related to Experimental Procedures.

Antibody	Source	Cat#
Chicken Anti-GFP Antibody	Thermo Fisher Scientific	A10262
Mouse Anti-GFP Antibody	Millipore	MAB3580
Mouse Anti-GFP Antibody (Living Colors A.v. Monoclonal Antibody JL08)	Clontech	632380
Rabbit Anti-RFP Antibody	MBL	PM005
Sheep Anti-Alpha-Melanocyte Stimulating Hormone Antibody	Chemicon	AB5087
Rabbit Melanin Concentrating Hormone Antibody	Phoenix Pharmaceuticals	H-070-47
Rabbit Anti-Phospho-p44/42 MAPK (Erk1/2) (Thr202/Tyr204) Antibody	Cell Signaling	4370
Goat Anti-mouse IgG Biotinylated Antibody	Vector Laboratories	BA-9200

Supplemental Experimental Procedures

BAC recombination, plasmid construction and generation of transgenic zebrafish lines

The BAC clones CH211-133P19, and DKEY-29L4 containing the *pomca* and *sst1.1* gene loci, respectively, were used for BAC recombination. PCR products of EGFPras-KanR and KaITA4-KanR cassettes flanked by homology arms for insertion at the start ATG of *pomca* or *sst1.1* were derived from pPCR-EGFP-KanRand pPCR-KaITA4-KanR plasmids, respectively (for primer sequences see Table S1). For generation of pPCR-EGFPras-KanR a Ras tag was fused to the EGFP coding sequence of pPCR-EGFP-KanR by a site directed mutagenesis PCR. For generation of pPCR-KaITA4-KanR, the KaITA4 cassette was removed from pCSKalTA4GI (Distel et al., 2009) by an *Eco*RI/*Hpa*I digest and inserted into pPCR-GFP-KanR from which the EGFP cassette was removed by an *Eco*RI/*Sna*BI digest. In addition, iTol2-Amp cassettes were placed in the vector backbones of BACs CH211-133P19 (pTARBAC2.1) and DKEY-29L4 (pIndigoBAC). iTol2-Amp cassettes flanked by homology arms for insertion into the respective BAC vector backbones were generated by amplification from pPCR8GW-itol2-Amp plasmid (Suster et al., 2009) using pTarbac2.1_iTol2-hom or pIndigoBAC_iTol2-hom primers (Table S1). BAC recombinations were performed using the pRed/ET technique according to manufacturer protocols (Quick & Easy BAC Modification Kit, Gene Bridges).

The plasmid for generation of the *Tg(pomca(pit):CFP-nfsb;cmlc2:GFP)*^{fr41Tg} line was cloned using the Gateway Tol2 kit (Kwan et al., 2007). For generation of p5E-pomca(pit), the pituitary specific *pomca* promoter (Liu et al., 2003) was amplified from genomic DNA, subcloned, re-amplified to add attB4-B1r attachment sites and inserted into pDONRP-P1R via a BP reaction. pME-CFP-nfsb was generated by addition of attB1-B2 attachment sites to a CFP-nfsb fusion construct via PCR followed by a BP reaction (for primers see Table S2). Finally, p5E-pomca(pit), pME-CFP-nfsb and p3E-pA (Kwan et al., 2007) were cloned into the destination vector pDestTol2CG2 (Kwan et al., 2007) via LR reaction. Stable transgenic lines were generated by standard injection and screening procedures.

Generation of R26-fl-rxΔ-ZsGreen mice

The SERCA ROSA26 targeting vector (Belgardt et al., 2008) was modified such that

the FRT-flanked IRES GFP cassette was replaced by a 2A-NLS-ZsGreen via *Asc*I/*Sma*I restriction and that a rox-flanked stop cassette was inserted into the *Asc*I site. Briefly, ZsGreen was amplified from pIRES2-ZsGreen1 vector (Clontech), using primers 5Asc2aZsGreen and 3SmaZsGreen (see Supplemental Table S3 for sequences), and verified by sequencing. Subsequently, a rox-flanked stop cassette (Anastassiadis et al., 2009) was amplified from SERCA using primers 5Mluroxwss 3Ascroxwss (see Supplemental Table S3 for sequences) and inserted 3' of the existing loxP-flanked neo stop cassette (Lasko et al., 1992) using *Asc*I and *Mlu*I/*Asc*I digestion. The resulting rosa26 targeting vector named B9-36 was linearized by *Asi*SI and 40 µg were transfected into C57BL/6-derived Bruce4 ES cells. Correctly targeted clones were identified by southern blotting on *Eco*RI-digested clonal DNA using the ROSA26 *Eco*/*Pac* and neo probes respectively. ES cells were injected into CB20 blastocysts to generate chimeric mice that were backcrossed to C57BL/6 animals to obtain germline transmission of the R26-fl-rx-ZsGreen allele. These mice were crossed with CAGGS Dre mice (Anastassiadis et al., 2009) to remove the rox-flanked stop cassette to obtain R26-fl-rxΔ-ZsGreen allele in which a loxP site-flanked neo stop cassette prevents expression of 2A-NLS-ZsGreen from the CAG promoter.

Sst-IRES-Cre; R26-fl-rxΔ-ZsGreen double transgenic mice were obtained by crossing homozygous R26-fl-rxΔ-ZsGreen mice to hemizygous Sst-IRES-Cre mice, yielding approximately 50% double transgenics with ZsGreen-labelled Sst cells. Genotyping was performed by PCR. The following primers were used for Sst-IRES-Cre: WT: 5’-CTGCAGTTCGATCACTGGAAC-3’ (forward), 5’-AAAGGCCTCTACAGTCTATAG-3’ (reverse), yielding 542 bp band; mutant: 5’-TCCAATTTACTGACCGTACA-3’ (forward), 5’-TCCTGGCAGCGATCGCTATT-3’ (mutant), yielding 450 bp band. The following primers were used for R26-fl-rxΔ-ZsGreen: 5’-AAAGTCGCTCTGAGTTGTTATC-3’ (shared forward), 5’-GATATGAAGTACTGGGCTCTT-3’ (reverse WT), 5’-TGTCGCAAATTAACTGTGAATC-3’ (reverse mutant). The WT allele gave a 570 bp band, the mutant allele a 380 bp band.

Electrophysiology

Perforated patch clamp experiments were performed on coronal brain slices (250-300 µm) from female and male $Sst^{ZsGreen}$ mice (6-9 weeks of age), which contained the PeVN. Experiments were carried out essentially as described previously (Hess et al., 2013; Könner et al. 2011). PeVN somatostatin neurons were identified according to their anatomical location and reporter expression. The brain slices were continuously superfused with carbogenated artificial cerebrospinal fluid (aCSF) (~31°C) at a flow rate of ~2 ml/min (recording chamber volume: ~2 ml). aCSF contained (in mM): 125 NaCl, 2.5 KCl, 2 $MgCl_2$, 2 $CaCl_2$, 1.2 NaH_2PO_4, 21 $NaHCO_3$, 10 HEPES, 5 glucose, adjusted to pH 7.2 with NaOH, resulting in an osmolarity of ~310 mOsm. Recordings were performed with pipette solution containing 1% biocytin (Sigma) and (in mM): 128 K-gluconate, 10 KCl, 10 HEPES, 2 $MgCl_2$, and adjusted to pH 7.3 with KOH. Initially, the patch pipette was tip filled with internal solution and back filled with 0.02% tetraethylrhodamine-dextran (D3308, Invitrogen, Eugene, OR, USA) and amphotericin B-containing internal solution (200 µg/ml; A4888, Sigma) to achieve perforated patch recordings (Horn and Marty, 1988; Akaike and Harata, 1994). Amphotericin B was dissolved in dimethyl sulfoxide (DMSO; final concentration 0.4–0.5%; D8418, Sigma) as described previsously (Rae et al., 1991) and was added to the modified pipette solution shortly before use. To block GABAergic and glutamatergic synaptic input the aCSF contained 10^{-4} M picrotoxin (P1675; Sigma-Aldrich), 5 x 10^{-5} M D-AP5; A5282; Sigma-Aldrich), and 10^{-5} M CNQX (C127; Sigma-Aldrich). αMSH (M4135; Sigma-Aldrich) was added to the aCSF at a concentration of 250 nM for durations of 5-7 min, as previously described (Ghamari-Langroudi et al., 2011). To analyze the αMSH responsiveness, the neuron's firing rate averaged from 10 sec intervals was taken as one data point. To determine the mean firing rate and standard deviation, 12 data points were averaged. On the single cell level a neuron was considered αMSH-responsive if the change in firing induced by αMSH was 3 times larger than the standard deviation (Dhillon et al., 2006; Kloppenburg et al., 2007).

In situ hybridization, immunolabelling and Nile Red staining of zebrafish larvae

Whole-mount fluorescent *in situ* hybridization, and whole-mount immunofluorescence staining (IF) of zebrafish were carried out as described (Filippi et al., 2007). To

increase signal intensity, *in situ* hybridization buffer was supplemented with 5-10% dextran sulfate (Sigma-Aldrich). DIG labeled probes for *pomca*, *gh1*, *oxt*, *trh*, *crh* and *sst1.1* were prepared as previously reported (see www.zfin.org). For generation of *mc4r* probes, partial coding sequences were cloned into pCRII (Invitrogen) and transcribed (sequence information available on request).

For information on antibodies used for zebrafish immunohistochemistry or immunofluorescence, see Table S6. Species-specific secondary antibodies coupled to Alexa Fluor 488 or 555 (Thermo Fisher Scientific) were used for IF experiments. Nuclear counterstaining was performed with DAPI (Thermo Fisher Scientific). For non-fluorescent immunostaining, samples were processed with standard protocols for DAB staining with the Vectastain Elite ABC-Peroxidase Kit (Vector Laboratories) using mouse anti-GFP primary (Millipore) and goat anti-mouse IgG biotinylated secondary antibodies (Vector Laboratories). For sections of DAB immunostained larvae or juvenile brains, samples were embedded in Durcupan (Sigma-Aldrich) and sectioned at a microtome (20 µm). For Durcupan embedding, larvae were dehydrated with increasing concentrations of Ethanol, then washed twice with acetone and incubated overnight in an acetone:Durcupan (1:1) mix. In turn, samples were transferred to sectioning molds containing pure Durcupan and incubated at 65°C until hardened. Cryo-sections (12 µm) of heads from juvenile fish and subsequent immunohistochemistry was performed as reported (Uribe and Gross, 2007).

RNAscope on mouse brain sections

Mice (n=5; 12 weeks of age) were perfused transcardially using a 0.9% saline solution at room temperature and fixed with 4% paraformaldehyde (pH 7.4) at 4°C. The brains were dissected and post-fixed for 18 h in 4% paraformaldehyde (pH 7.4) at RT. The solution was changed to 25% sucrose in 0.1 M PBS (pH 7.4) and incubated overnight at 4°C. The brains were cut at a freezing microtome. The brain sections were 14 µm thick and were collected in a 30% ethylene glycol and 20% glycerol in PBS solution. On the day before the assay, every 8th section throughout the PVN and PeVN was mounted on SuperFrost Plus Gold slides (Thermo Fisher Scientific) and incubated overnight at 60°C. One section from each animal was mounted to be used as negative control. Fluorescent *in situ* hybridization for Sst and Mc4r mRNA detection was performed using RNA scope technique. Reagents were

purchased from Advanced Cell Diagnostics (Hayward, CA), if not mentioned otherwise. In brief, sections were pre-treated for 10 min in hydrogen peroxide (Cat# 322381) at RT, followed by submersion in Target Retrieval (Cat# 322000) for 8 min at 98-99°C. The slides were rinsed twice in autoclaved Millipore water and quickly dehydrated in 100% ethanol. After air drying, a hydrophobic barrier was made around the sections using an ImmEdge hydrophobic barrier pen. The incubations were performed at 40°C, using the HybEz Hybridization System for Manual Assays. Sections were incubated for 40 min with protease III (Cat# 322381), followed by probe hybridization for 2 h. C1-probe for MC4R, no dilution, (Cat# 402741) and C3-probe for Sst (Cat# 404631-C3), diluted 1:50, were used. A 3-plex positive (Cat# 320881) and a 3-plex negative (Cat# 320871) control probes were processed in parallel with the target probes to assess the quality of the assay. Probe hybridization was followed by 2x2 min washes in Wash buffer (Cat# 310091). The manufacturer protocol for RNAscope® Multiplex Fluorescent v2 Assay (Cat# 323110) was followed for the remaining steps (amplification and detection). Briefly, AMP1 and AMP2 were incubated for 30 min, followed by AMP3 incubation for 15 min. Between each amplification step, 2x2 min washes were performed. Afterwards a TSA Plus amplification (Perkin Elmer, Cat# NEL760001KT) protocol was used. C1-probe tyramide fluorophore was Cy3 and C3-probe fluorophore was Fluorescein. DAPI was used for counterstaining and ProLong® Gold Antifade Mountant (Thermo Fisher Scientific, Cat# P36931) was used to coverslip the sections.

Imaging and quantitative evaluations of fluorescent images

Confocal z-stacks of zebrafish fluorescences were recorded using a Zeiss LSM 710 microscope. For confocal imaging, whole larvae were mounted in 80% glycerol containing 1.2 % low melting agarose/PBS. Juvenile brains or brain hemispheres were mounted in 80% glycerol in PBS only. Brains of DiI injected samples were imaged in PBS without optical clearing to avoid dye diffusion. Light microscopy was performed at a Zeiss M2 compound microscope for which samples were mounted in 80% glycerol/PBS. Cryo-sections were covered with Mowiol mounting medium. Imaging of whole larval brains at 7 dpf or older stages required careful removal of all ventral tissue underneath the skull in order to optimize optical quality. For image processing, ZEN (Zeiss), Photoshop CS2 (Adobe) and Fiji (Image J, NIH) softwares were used. Optical midline sections were generated with Imaris (Bitplane).

Imaging of mouse RNAscope labelings was performed at a Leica TCS SP-8-X confocal microscope. Tile scans and Z-stacks (optical section of 1.0 µm) of the PeVN were captured. Laser intensities for the two probe channels were kept constant throughout the entire material. Images were imported into FIJI software (NIH) where maximum intensity projections were generated.

For measurement of pERK levels in Pomca or Sst1.1 neurons of *Tg(pomca:EGFPras)*^{fr38Tg} or *Tg(sst1.1:EGFPras)*^{fr40Tg} transgenic zebrafish, respectively (Figures 2G,H and 7E), samples were subjected to immunostaining for GFP (Chicken Anti-GFP Antibody, Thermo Fisher Scientific; secondary antibody A488 coupled) and pERK (rabbit Anti-pERK Antibody, Cell Signaling; secondary antibody A555 coupled). Following staining, the samples of pharmacologically treated and control groups were imaged at a confocal microscope with identical acquisition settings. Z-axis distance of single focal planes was 1.5 µm. Scanned raw images were in turn processed using a MATLAB-based image segmentation algorithm (Fluo_traces_v2.m) according to published protocol (Wong et al., 2010). For pERK levels of *sst1.1:EGFPras* cells, an average of 73 ± 19 cells per brain hemisphere derived from seven brains were used for quantification. For pERK levels of *pomca:EGFPras* cells, 119 (ND saline), 54 (ND leptin), 57 (HD/HF saline) and 81 (HD/HF leptin) individual Pomca neurons derived from 4 brains per group were used for quantifications.

For quantification of axonal innervation of the preoptic area in zebrafish larvae (Figure 3K,L), confocal z-stacks (1 µm optical sections) of anti-GFP IF processed *Tg(pomca:EGFPras)*^{fr38Tg} larvae were generated (see Figure S4). Automatic quantification of axon numbers was performed according to the following protocol using Fiji software: Image sequences were loaded into Fiji. As a region of interest, a single line was chosen perpendicular to the axon tract crossing the preoptic area (middle distance between anterior and posterior commissures), or perpendicular to the tract of the anterior commissure (at the level of the midline). Using the „Reslice“ tool, optical cross sections were generated and single axons were quantified using the „Find Maxima“ function of Fiji. For n numbers see respective Figure Legends.

For quantification of DAPI-, Sst- and Mc4R-positive cells in the mouse PVN (Figure 6F), images were imported and fused into Halo software (Indica Labs). Cell identification was obtained based on DAPI staining, and the presence of 3-5 dots per

cell was used as threshold for probe recognition. Only cells with labelling above this threshold were considered positive. Absolute numbers of DAPI-, Sst- and Mc4R-positive cells were determined for equivalent, equally-sized and manually defined rectangular areas of the PeVN, and Sst/DAPI and Mc4R/DAPI ratios were calculated from these absolute numbers.

Supplemental References

Akaike, N., and Harata, N. (1994). Nystatin perforated patch recording and its applications to analyses of intracellular mechanisms. Jpn J Physiol *44*, 433-473.

Anastassiadis, K., Fu, J., Patsch, C., Hu, S., Weidlich, S., Duerschke, K., Buchholz, F., Edenhofer, F. and Stewart, A. F. (2009) Dre recombinase, like Cre, is a highly efficient site-specific recombinase in E. coli, mammalian cells and mice. Dis Model Mech. *2*, 508-515

Belgardt, B. F., Husch, A., Rother, E., Ernst, M. B., Wunderlich, F. T., Hampel, B., Klöckener, T., Alessi, D., Kloppenburg, P. and Brüning, J. C. (2008). PDK1 deficiency in POMC-expressing cells reveals FOXO1-dependent and -independent pathways in control of energy homeostasis and stress response. Cell Metab *7*, 291-301.

Distel, M., Wullimann, M.F., and Köster, R.W. (2009). Optimized Gal4 genetics for permanent gene expression mapping in zebrafish. Proc Natl Acad Sci U S A *106*, 13365-13370.

Dhillon, H., Zigman, J. M., Ye, C., Lee, C. E., McGovern, R. A. , Tang, V. , Kenny, C. D., Christiansen, L. M., White, R. D. , Edelstein, E. A. , Coppari, R., Balthasar, N., Cowley, M. A. , Chua, S. Jr, Elmquist, J. K. and Lowell, B. B. (2006). Leptin directly activates SF1 neurons in the VMH, and this action by leptin is required for normal body-weight homeostasis. Neuron *49*, 191-203.

Filippi, A., Durr, K., Ryu, S., Willaredt, M., Holzschuh, J., and Driever, W. (2007). Expression and function of nr4a2, lmx1b, and pitx3 in zebrafish dopaminergic and noradrenergic neuronal development. BMC Dev Biol *7*, 135.

Horn, R., and Marty, A. (1988). Muscarinic activation of ionic currents measured by a new whole-cell recording method. J Gen Physiol *92*, 145-159.

Kloppenburg, P., Zipfel, W. R., Webb, W. W. and Harris-Warrick, R.M. (2007). Heterogeneous effects of dopamine on highly localized, voltage-induced Ca2+ accumulation in identified motoneurons. J Neurophysiol *98*, 2910-2917.

Kwan, K.M., Fujimoto, E., Grabher, C., Mangum, B.D., Hardy, M.E., Campbell, D.S., Parant, J.M., Yost, H.J., Kanki, J.P., and Chien, C.B. (2007). The Tol2kit: a multisite gateway-based construction kit for Tol2 transposon transgenesis constructs. Dev Dyn *236*, 3088-3099.

Lakso, M., Sauer, B., Mosinger, B. Jr, Lee, E. J., Manning, R. W., Yu, S. H., Mulder, K. L. and Westphal, H. (1992). Targeted oncogene activation by site-specific recombination in transgenic mice. Proc Natl Acad Sci U S A. *8*9, 6232-6236.

Liu, N.A., Huang, H., Yang, Z., Herzog, W., Hammerschmidt, M., Lin, S., and Melmed, S. (2003). Pituitary corticotroph ontogeny and regulation in transgenic zebrafish. Mol Endocrinol *17*, 959-966.

Rae, J., Cooper, K., Gates, P. and Watsky, M. (1991). Low access resistance perforated patch recordings using amphotericin B. J Neurosci Meth *37*, 15–26.

Suster, M.L., Sumiyama, K., and Kawakami, K. (2009). Transposon-mediated BAC transgenesis in zebrafish and mice. BMC Genomics *10*, 477.

Wong, L.C., Lu, B., Tan, K.W., and Fivaz, M. (2010). Fully-automated image processing software to analyze calcium traces in populations of single cells. Cell Calcium *48*, 270-274.